Spatially-structured cell populations process multiple sensory signals in parallel in intact vascular endothelium

Matthew D. Lee[1], Calum Wilson[1], Christopher D. Saunter[2], Charles Kennedy[1], John M. Girkin[2] & John G. McCarron[1*]

[1]Strathclyde Institute of Pharmacy and Biomedical Sciences, University of Strathclyde, 161 Cathedral Street, Glasgow G4 0RE, UK. [2]Centre for Advanced Instrumentation, Biophysical Sciences Institute, Department of Physics, Durham University, South Road, Durham, DH1 3LE, UK.

Short Title: Stimulus-specific sensory cells in the intact vascular endothelium

*author for correspondence

The vascular switchboard. The endothelium is exposed to a constant cacophony of simultaneous instructions from hormones, neurotransmitters, pericytes, smooth muscle cells, various blood cells, viral or bacterial infection and proinflammatory cytokines. It is often assumed that the endothelium maximizes the ability of tissues to respond to instructions through coordinated responses in a homogeneous population of cells. We show that the endothelium segregates chemical environment into separate, complementary streams of information that are processed in parallel, providing separate lines of information about the chemical environment like a vast switchboard. Different, simultaneously arriving, inputs are passed among cells and computations carried out so that a new signal output is generated that is a composite of the inputs. The endothelium detects specific signals in a complex chemical environment by using cells that are not concerned with all possible available information but with only with a small specific part of the overall material and cells collaborate with neighbors in the distribution of information.

Abstract

Blood flow, blood clotting, angiogenesis, vascular permeability and vascular remodeling are each controlled by a large number of variable, noisy and interacting chemical inputs to the endothelium. The endothelium processes the entire chemical composition to which the cardiovascular system is exposed, carrying out sophisticated computations to determine physiological output. A major challenge faced by the endothelium is the requirement to process an enormous quantity of information held in the overall chemical environment to which the vascular system is exposed. We analyzed hundreds of endothelial cells and show that the endothelium segregates the chemical environment into small components of complementary information streams which are processed in parallel. Chemical stimuli arriving at the endothelium are mapped to different clusters of cells which each generate unique signal patterns. When there is more than one stimulus, cells communicate and combine inputs across information streams to generate new distinct signals. Our results establish the endothelium is a structured, collaborative, sensory network which simplifies the complex environment using separate cell clusters concerned with small distinct aspects of the overall information. These clusters interactively compute signals from the diverse but interrelated chemical inputs. These features permit the endothelium to selectively process separate signals and perform multiple computations in an environment that is noisy and variable.

Introduction

The endothelium is a continuous network of ten trillion cells (*1*) that controls virtually all cardiovascular behavior. The endothelium is the sensory interface for an enormous quantity of information held in the chemical environment to which the vascular system is exposed and which provides cues on physiological status. Numerous signals are provided by blood composition, hormones, neurotransmitters, endothelial cells, pericytes, smooth muscle cells, various blood cells, viral or bacterial infection and proinflammatory cytokines that each provide instructions to the vascular system. Many (minimally tens) of these extracellular signals may arrive simultaneously, often fluctuating around basal concentration values creating multiple, small, difficult to resolve extracellular signals (*2-5*). The endothelium processes the information held in the identity of the chemical activator and in the range of concentrations over which each fluctuates. The endothelium must manage multiple extracellular signals simultaneously requiring selective detection and processing of separate information.

Although heterogeneity is appreciated to exist (*6-9*), the endothelium is usually treated as a homogeneous population of cells that responds uniformly to each activator. Indeed, it has often been assumed that biological systems maximize tissues' ability to respond to perturbations through coordinated responses in homogeneous population of cells (*10*). The classical view of endothelial function is that information arriving via each cell is interpreted and conveyed to neighboring cells (e.g. other endothelial cells or smooth muscle), much like a cable, without changing the information content (*11, 12*). Given this proposed arrangement, precisely how the endothelium transduces multiple independent extracellular signals arriving simultaneously, to particular cell activities is not clear.

Chemical stimuli that activate endothelial cells are often transduced to changes in cytosolic Ca^{2+} concentration (*13-19*) (but see *20*). Ca^{2+} links extracellular stimuli to physiological response by regulating the synthesis and release of various vasoactive agents such as nitric oxide, prostacyclin, peptides and thromboxane (reviewed *21*). Through these Ca^{2+}-dependent mediators the endothelium controls vascular tone, nutrient exchange, blood cell recruitment, blood clotting and the formation of new blood vessels (reviewed *21*). Cardiovascular function requires careful translation of the physiological information provided by extracellular activators, via changes in intracellular Ca^{2+}, to regulate both single cell activity and the physiological

behavior of the entire endothelium. Translation occurs when the activity of intracellular processes alter in response to the Ca^{2+} signal. Specific targeting of particular intracellular processes by extracellular signals is believed to rely mainly on differentiation based on amplitude or temporal or spatial features of the Ca^{2+} signal within each cell (*22-25*). However, despite the diversity of signals, various activators evoke Ca^{2+} increases that often appear similar in their localized increases, uniform global rises or propagating waves that occur through all or part of a cell (*26-29*). How these Ca^{2+} signals selectively evoke a multitude of distinct physiological responses is not yet fully understood.

When several chemical mediators are present simultaneously, the Ca^{2+} signal must integrate information from each source while still producing distinct signals to control multiple activities thus presenting an additional complex sensory problem. An appreciation of how Ca^{2+} selectively couples different sensory inputs in a complex chemical environment to various physiological functions is therefore central to an understanding of endothelial functioning.

To control cardiovascular function the endothelium extracts information from a noisy and variable environment by performing multiple simultaneous determinations of chemical signals via changes in Ca^{2+} concentration to determine physiological status. Key to an understanding of this crucial aspect of the cardiovascular function are the mechanisms by which endothelial cells integrate information from the local chemical environment. To address this issue we recorded the concurrent activity from hundreds of endothelial cells in intact blood vessels and examined the responses to extracellular activators of muscarinic and purinergic receptors. The response to muscarinic receptor activation is thought to underlie the response hypothermia (*30*) and to shear-stress activation (*31*). Purinergic stimulation may occur by ATP released from activated platelets (*32, 33*) to evoke vasodilation (*34*) and either an increase (*35*) or decrease (*36*) in endothelial permeability.

Our results show the endothelium is organized into spatially-structured clusters of endothelial cells. The clusters focus on particular stimuli and separately process various elements of the chemical environment in parallel. Cells share information with neighbors. When more than one agonist is present, cells perform computations on inputs to generate new signals that are distinct from each of the individual contributions. The endothelium thus appears to act as a network of

structured, collaborating sensors that act in parallel to interpret the multiple signals that report physiological status.

Results

The endothelium is a distributed sensory system that can detect a large number of chemical inputs (*21, 37*). However, it is not known if the distribution of sensory cells is uniform, random or clustered. As a first step in determining the distribution of sensory cells and how the endothelium responds to extracellular activators, agonist-induced Ca^{2+} signaling was studied in large numbers (~200) of endothelial cells in intact arteries.

The muscarinic agonist carbachol (CCh; 100 nM) evoked an increase in Ca^{2+} concentration in several cells in the endothelium (Fig 2A; supplementary fig S1). The cells that activated appeared to form clusters in certain areas of the endothelium (Movie S1). Each active cell's response consisted of Ca^{2+} waves that propagated across all or part of the cell (Movie S1). Some cells were inactive or barely active and others highly active with repeating Ca^{2+} waves and oscillations (Fig 2A-F). The amplitude and duration of the responses also varied across cells (Fig 2C,D). The differences in amplitudes, duration and oscillation frequency from individual cells gave rise to a wide range of responses (Fig 2A,C,D). There also was considerable heterogeneity in the response to other types of activator including the flow-induced responses in the endothelium (supplementary fig S2). Despite the wide variation in amplitudes, durations and oscillations, when the response to CCh was averaged across all cells or the entire field of view, a monophasic rise in Ca^{2+} occurred (supplementary fig S1F).

CCh-evoked changes in endothelial Ca^{2+} were required for relaxation of the arteries. When Ca^{2+} changes in the endothelium were buffered using the chelator BATPA (30 μM perfused into the artery lumen for 30 min), the relaxation evoked by a maximal concentration of carbachol (100 μM) was inhibited (supplementary Fig S3).

Concentration-dependence of cholinergic signaling

Previous studies have shown the averaged or ensemble endothelial Ca^{2+} response to various stimuli increased in a concentration dependent manner (*16, 38*). However, it was not clear if these increases in response arose from an increase in the Ca^{2+} response in each single cell or an increase in the number of cells being activated (each responding with a maximum response); single cell concentration-response relationships are rarely carried out. Figure 2A shows that the number of cells responding with Ca^{2+} elevations, increased with CCh concentration. The cells

that activated to each concentration appeared to be positioned in clusters in various areas of the endothelium. The range (EC_{10}-EC_{90}) of CCh concentrations over which cells responded was 123 nM – 1.2μM (95% confidence intervals: 76 – 199 nM for EC_{10}; 740nM – 2.1 μM for EC_{90}; Fig 4D). This data indicates at least part of the concentration dependence of the response to muscarinic activation arises from increased recruitment of endothelial cells.

In addition to the increased recruitment of cells, the amplitude of the Ca^{2+} response in each cell also increased in a concentration-dependent manner (Fig 4C,E). The half-maximal concentration of CCh for endothelial cell activity was 630 nM (95% confidence interval: 399 nM – 996 μM; supplementary Fig S4). The range (EC_{10}-EC_{90}) over which the magnitude of the Ca^{2+} response, of responding cells, increased was 50 nM – 8 μM (95% confidence intervals: 17 nM – 142 nM for EC_{10}; 2.9 μM – 22.1 μM for EC_{90}; supplementary Fig S4). Thus the concentration-dependent response was a combination of increasing recruitment of cells and increasing amplitude of response within cells (supplementary Fig S4).

There were differences in the sensitivities of concentration-responses in amplitude and number of cells activated (supplementary fig S4). All cells could be activated before a maximal response was achieved as expected from a population of cells with various sensitivities (supplementary fig S4). A composite measure (supplementary fig S4) of the percentage cells activated multiplied by the average amplitude of the initial Ca^{2+} rise in responding cells, at each concentration shows the half-maximal concentration of CCh for *total* endothelial activation was 1.1 μM (95% confidence interval: 743 nM – 1.5 μM). The range (EC_{10}-EC_{90}) of concentration of CCh over which cells responded was 164 nM – 6.8 μM (95% confidence intervals: 76 nM – 354 nM for EC_{10}; 3.2 μM – 14.8 μM for EC_{90}). The concentration response relationship for total endothelial response (supplementary fig S4) was significantly right-shifted compared to the relationship describing percentage cell activation supplementary fig S4 versus Fig 4D; $P<0.05$). Thus, the concentration-dependence of the response of individual cells extends the overall sensitivity of the endothelium.

The Ca^{2+} increase evoked by CCh was generated via muscarinic receptors as confirmed by the complete block of the response by the M3 receptor antagonist 4-DAMP (100 nM; Fig 3). The experiment shown in Fig 3A-D begins with repeat activations with CCh (10 min between activation) to show reproducible responses. The M3 receptor antagonist (4-DAMP 100 nM) was

then applied and blocked the subsequent response to CCh. After block of the CCh response by the antagonist, ATP (100 μM) was applied to confirm viability of the endothelium (Fig 3A-D)

Concentration-dependence of purinergic signaling

In the next series of experiments, the response to the purinergic agonist ATP was examined (Fig 4A). Ca^{2+} responses, averaged across all endothelial cells within the field-of-view, showed a concentration-dependent increase in magnitude of response (Fig 4B). The increasing response to ATP was, like CCh, derived from an increased number of cells activated and an increased amplitude of response in each cell (Fig 4A-E). The cells that activated to each concentration appeared to be positioned in clusters in various areas of the endothelium (Fig 4A).

The half-maximal concentration of ATP for cell activation was 3.17 μM (95% confidence interval: 2.19 μM – 4.58 μM; Fig 4D). The range (EC_{10}-EC_{90}) of concentration of ATP over which cells responded was 438 nM – 22.9 μM (95% confidence intervals: 196 nM - 979 nM for EC_{10}; 10.2 μM – 51.2 μM for EC_{90}; supplementary fig S5).

When the magnitude of the peak response was considered, the half-maximal concentration of ATP was 20.5 μM (95% confidence interval: 12.2 μM to 34.3 μM; supplementary fig S5). The range (EC_{10}-EC_{90}) for the magnitude of the Ca^{2+} response was 1.9 μM to 224 μM (95% confidence intervals: 590 nM - 5.9 μM for EC_{10}; 71.2 μM – 700 μM for EC_{90}).

When a composite measure of the percentage cells activated, multiplied by the average amplitude of the initial Ca^{2+} rise, is assessed (supplementary fig S5), the half-maximal concentration of ATP for *total* endothelial activation was 21.4 μM (95% confidence interval: 13.9 μM – 33.0 μM). The range (EC_{10}-EC_{90}) of concentration of ATP over which cells responded was 2.6 μM – 174 μM (95% confidence intervals: 1.0 μM – 6.7 μM for EC_{10}; 68.1 – 488 nM for EC_{90}; supplementary fig S5). The concentration response relationship for the total endothelial response was, like CCh, significantly right-shifted compared to the relationship describing percentage cell activation ($P<0.05$). Thus, as with muscarinic activation, whilst there is only a narrow range of concentrations over which the endothelium as a whole responds to ATP, the concentration-dependence of the response of individual cells extends the overall sensitivity of the endothelium.

Activation of purinergic receptors by ATP respectively evoked relaxation of intact arteries. The relaxation evoked by ATP (100 μM), like that of CCh, required Ca^{2+} changes in the endothelium. When Ca^{2+} changes were buffered in the endothelium using the chelator BATPA (30 μM perfused into the artery lumen for 30 min), the relaxation evoked by a maximal concentration of ATP was blocked (supplementary Fig S3).

The response to ATP was mediated by purinergic P2Y2 receptors. Two observations support this conclusion. First, the Ca^{2+} rise to ATP persisted in a Ca^{2+}-free bath solution (Fig 5). In response to the ATP (EC_{25}) the response was unaltered when extracellular Ca^{2+} was removed (Fig 5A-C). At a maximal ATP concentration (100 μM) the initial response was unaffected in a Ca^{2+}-free bath. However, the later (45 s) sustained response to ATP was reduced suggesting that Ca^{2+} influx was required for this part of the ATP evoked Ca^{2+} rise (Fig 5F-H). Ca^{2+} influx in the later sustained responses appears to arise from store-operated Ca^{2+} entry rather than P2X receptor activation (see below).

The second line of support for P2Y2 receptor involvement is that the responses to a maximal concentration (100 μM) of ATP (both initial and sustained) were largely blocked by the P2Y2 receptor blocker ARC118925 (1 μM; 0.61±0.13 versus 0.13±0.06; Fig 6A). The small residual component for the response to ATP, after ARC118925, was blocked by the P2Y1 receptor antagonist (MRS2179, 10 μM; Fig 6A). The P2Y1 receptor antagonist MRS2179 had only a small inhibitory effect on the response to ATP (10 μM; 66% of controls 0.61±0.13 versus 0.4019±0.09) (Fig 6).

The almost complete block of the response to ATP by the P2Y2 antagonist suggests that the sustained part of the response involved store-operated Ca^{2+} entry rather than P2X receptor activation.

Distribution of Sensitivities among cells to puringeric and muscarinic activation

We next addressed the distribution of cells that were most sensitive to CCh and ATP. The concentration at which 25% and 75% of the cells responded to each agonist (EC_{25} and EC_{75}) were obtained from the concentration response curves (Fig 2D & Fig 4D) and used to determine which cells were activated by low and high concentration of each agonist. The experiments examining each agonist were carried out on precisely the same preparation and field of

endothelial cells and show each agonist activates different spatially-distinct cells. In examining the different populations of cells activeated by each agonist, we restricted our analysis to the first 4 seconds of activation to minimize Ca^{2+} waves moving from an activated cell (*39*).

Fig 7A shows the cells activated by the EC_{25} and EC_{75} of CCh and ATP in a single endothelial preparation. A low concentration of CCh (EC_{25}) produced an initial response in a small percentage of endothelial cells (Fig 7Ai; n=5). Additional cells are subsequently recruited either by the agonist or by the Ca^{2+} increase in the initial responding cells propagating to neighboring cells (Fig 7Aii). The EC_{75} concentration of CCh also evoked a response in those cells that responded to the EC_{25} of CCh (Fig 7Ai first responding and 7Aii full response). However, more initial responders were activated by higher concentrations of the agonist (Fig 7Ai) and further cells were subsequently recruited. The EC_{25} and EC_{75} of ATP also produced a similar concentration-dependent activation of cells (Fig 7Ai & 7Aii). Cells that activated to the same agonist appeared to form clusters and the clusters activated by CCh were spatially-distinct from those cells activated by ATP (Fig 7A&B; Movie S2).

The cells activated by each agonist were highly reproducible and the same pattern of cell activity for each agonist occurred when the sequence of activation of activation was reversed (supplementary fig S6).

To provide a robust statistical description of cell spatial and neighbor relationships, we used a Voronoi tessellation analysis (Fig 7) (described in Methods). Analysis of the Voronoi plots provide a quantitative method to determine the number of neighbors of each cell, and the number of co-activating neighboring cells i.e. a method to determine the extent of clustering. The analysis was restricted to the first 4s of activation, a time long enough to identify the first responding cells and short enough to minimize activation of cell due to signal propagation (*39*). This approach was taken in preference to the use of Gap junction blockers as we previously found carbenoxalone, glycyrrhetinic acid and GAP-27 each suppressed Ca^{2+} signals in the endothelium independently of effects on Gap junctions (*8*). The present results show that each cell has on average 6 neighbors, CCh-sensitive cells tended to be close to other CCh sensitive cells and ATP-sensitive cells tended to be close to other ATP sensitive cells (Fig 7B).

Using Voronoi edge tessellation to define neighbors we determined the number of co-activating

neighbors responding to a given stimulus (Fig 7C,D). Thus for *every* activating cell, the number of neighbors cells that also activate to the same stimulus was determined. From this data a null hypothesis was generated to suggest that there is no spatial correlation in the responses, i.e. that a cell is no more likely to activate if its neighbor activates. The expected number of co-activating cells under the null hypothesis was calculated as the (mean number of neighbors; 6) * (activating fraction) for each agonist. As this hypothesis can be arrived at by assigning the response/no response behavior to cells in a spatially random way, we call this the 'random model'.

The number of neighboring endothelial cells activated by equivalent (EC_{25} & EC_{75}) concentrations of CCh and ATP (Fig 7C,D red dots) was significantly greater than predicted by the random model distribution of activated cells (Fig 7C,D blue dots), suggesting that cells that respond to each agonist tend to be neighbors and that cells are arranged in sensing clusters. The difference between the random model and observed response was greater in the first 4s of activation (Fig 7C) than the full duration data set (Fig 7D) presumably because cell-cell propagation increased the number of cells activated after this period and extended signals beyond the clusters.

We next analyzed the extent of overlap in clusters that were activated by each agonist. In this analysis the cells that respond to one agonist were first identified. Then the percentage of precisely the same cells that respond to the second agonist was determined (note that the EC_{25} and EC_{75} concentrations were derived from the concentration response data over the full duration of the response; Fig 4D & 7D). Summarized data (n=5) plotting the overlap in the cells activated by CCh and ATP during the first 4 seconds (first responding). The left side of the plot (Fig 7E; red) shows the total number of cells that have been activated as a percentage of the entire population of cells in the field by the condition in the red bar. The right side of each plot (Fig 7E) shows the percentage of the precisely the same cells identified on the left plot that are activated by each of the conditions shown on the x-axis. From this analysis it is clear that only a small percentage of cells that respond to CCh (EC_{25}) also respond to ATP (EC_{25}), and likewise that a small percentage of cells that respond to ATP (EC_{25}) also respond to CCh (EC_{25}).

Confirmation that cell activation tended to occur in clusters is shown in the summarized data in Fig 7F showing responses to CCh and ATP in the same population. Cluster sizes were measured by identifying interconnected cells from the Voronoi neighbor analysis. The number of cells in a

cluster (in the first 4s of activation) increased substantially with agonist concentration for CCh but the increase was much shallower for ATP (Fig 7F). This result suggests the extent of subsequent recruitment of cells after the first 4 s was substantially greater for ATP than CCh.

The question arises as to why some cells respond more to one agonist than another. At least part of the explanation appears to be the distribution of M3 and P2Y2 receptors. Fluorescence labelling of M3 and P2Y2 receptors shows the distribution is highly heterogeneous (Fig 8). Some cells show increased M3 receptor labelling while other cells more P2Y2 receptor labelling (Fig 8). Indeed, the cells that expressed M_3 receptors were spatially distinct from the cells that expressed $P2Y_2$ receptors with no significant overlap ($P<0.05$, n=5; Fig 8C,D). In these experiments cell boundaries were identified using PECAM-1 fluorescence. From the cell boundaries ROI's were extracted to identify individual endothelial cells.

The specificity of the P2Y2 antibody used in these experiments (Fig 8) was confirmed using wild-type 1321N1 cells and 1321N1 cells stably expressing recombinant human hP2Y2 receptors (1321N1-hP2Y2)(*40*) (supplementary Fig S7). 1321N1 cells are a human astrocytoma cell line that do not endogenously express any of the eight P2Y receptor subtypes or respond to the naturally-occurring nucleotide agonist (*41*) and were used as a negative control (supplementary fig S7). The P2Y2 antibody labelled 1321N1-hP2Y2 but not wild-type 1321N1 cells. The fluorescent ligand used to label M3 receptors was completely blocked by the M3 receptor antagonist 4-DAMP (Fig 8).

Heterogeneity in responses is not restricted to Ca^{2+}. In another series of experiments the spatial heterogeneity in nitric oxide production was examined using the fluorophore DAR-4M (*29*). The production of nitric oxide largely occurred in separate cells in response to an EC_{50} concentration (for Ca^{2+}) of CCh or ATP in the same preparation (supplementary fig S8). In this series of experiments, cells that generate nitric oxide to one agonist were first identified. Then the percentage of precisely the same cells that respond to one agonist was determined for the second agonist. Summarized data (n=3) is plotted showing the overlap in the cells activated by CCh and ATP (supplementary fig S8B-C). In supplementary fig S8B-C, the red bar shows the total number of cells that have been activated as a percentage of the entire population of cells in the field. The right side of each plot (blue bars) shows the percentage of the precisely the same cells that are activated by the agonists shown on the x-axis. There is a significant difference in the

cells that respond to each agonist i.e. there is minimal overlap in the percentage of cells that respond to CCh with nitric oxide production with those that respond also to ATP.

Together these results suggest clusters of cells have a higher sensitivity to muscarinic agonist while other, different clusters of cells have a high affinity for purinergic agonists. Thus the endothelium uses an agonist specific sensing systems for each agonist.

Characteristics of Ca^{2+} signals

The spatiotemporal features of the Ca^{2+} signals in response to low but equivalent concentrations (EC_{25}) of CCh and ATP, evoked in the same preparation, differed substantially (Fig 9A-D). In single endothelial cells, CCh (EC_{25}) evoked repetitive Ca^{2+} oscillations on an elevated baseline value (Fig 9B,C). The mean response from the activated cells (Fig 9B, green line) showed a slow, steady increase in Ca^{2+} which remained elevated throughout the treatment (Fig 9B). In contrast, a low concentration of ATP (EC_{25}) evoked a rapid rise in Ca^{2+} followed by a decline back to resting values (Fig 9B). Several cells showed repetitive oscillations (Fig 9B). The mean response to the EC_{25} of ATP (Fig 9B, red line) was a sharp increase in Ca^{2+} that subsequently declined to baseline levels (Fig 9B). When CCh and ATP (each at their EC_{25}) were applied together, the cells that responded to the combined treatment were the same cells that responded to the separate application of each agonist (Fig 9A).

Interestingly, when both agonists (CCh and ATP) were present, the Ca^{2+} responses appeared to be a composite of the amplitudes and temporal features of the signals derived from each agonist when they were applied separately (Fig 9B,C). Thus, when compared to the CCh alone response, there was a sharper increase in Ca^{2+} in responding cells followed by an elevated phase which had a higher amplitude than in CCh alone. [Ca^{2+}] remained elevated (Fig 9B, right plot).

The change in characteristics of the Ca^{2+} response occurred in individual cells (Fig 9C) i.e. the change was not a consequence of an analysis that averaged responses across cells. In Fig 9C the responses of 3 separate cells to CCh, ATP and both agonists are shown – it is the same 3 cells in each case. Cell 1 (Fig9C left-panel) responds to CCh but not to ATP. While the cell des not respond to ATP with a Ca^{2+} change, the characteristics of the response to CCh is altered when ATP is also present (combined) and there is a faster and larger upstroke. Cell 2 (Fig 9C middle-panel) responds to ATP but not CCh. The characteristics of the response in Cell 2 to ATP is

altered when CCh is also present (combined) and there is a smaller initial peak and a more sustained later Ca^{2+} change. Cell 3 (Fig 9C right-panel) responds to CCh and to ATP. Once again the characteristics of the response in Cell 3 is altered when ATP and CCh both are present. The reduced rapid initial spike to ATP, when both agonists were present, may have occurred because those cells that responded to ATP were sensitive to CCh though not Ca^{2+} responsive to the agonist.

The combined response that occurred when both agonists were present was neither the mean nor a linear summation of the individual responses. The mean peak to CCh and ATP when both agonists were present (combined) exceeded the mean response to CCh and ATP when they were applied separately and was less than the summed response (Fig 9D). The combined steady-state response exceeded both the mean and the summed response to the EC_{25} of CCh and ATP when applied separately (Fig 9E). These results suggest the precise nature of the computation carried out when both agonists are present is not clear but appears to be non-linear for both the peak and steady-state response and in the case of the steady-state response, expansive, in that the combined response exceeds linear summation of each input.

Communication among cells

The new composite Ca^{2+} signals that arose when both agonists were present may have occurred because cells are sensitive to both activators but sub-threshold to one or because signals from each agonist are communicated from other cells to the cell in which the composite behavior was seen. Both possibilities appear to exist.

To determine if communication occurred, we first identified cells that were largely unresponsive to one activator at each of the EC_{25} and EC_{75} concentrations from a field of endothelium (Fig 10A-D). Figure 10C,D shows an example cell in which the response to CCh at the EC_{25} or EC_{75} was small and had little concentration dependent increase indicating subthreshold behavior. This same cell responded strongly to ATP (Fig 10D). The response to ATP (EC_{25}) was a small Ca^{2+} peak which decline towards resting values. ATP (EC_{75}) evoked a larger transient rise, which declined to a small sustained elevation in baseline. Interestingly, while the cell responded weakly to CCh, nonetheless, CCh (EC_{25}) substantially altered the response to ATP (EC_{25}). At the EC_{25} of ATP when the CCh (EC_{25}) was also present, there was a larger and more sustained elevation in

Ca^{2+} with oscillations, than when ATP (EC_{25}) alone was present. Since responses to the EC_{25} and EC_{75} of CCh was at best weak, the modification of the response to ATP (EC_{25}), when the EC_{25} of CCh was present, is consistent with the cell responding directly to ATP (EC_{25}) while receiving signals from neighboring CCh-sensitive cells.

Some cells are sensitive to both activators. We found in those cells, the Ca^{2+} response was distinctive to each agonist (Fig 9C) i.e. CCh (EC_{25}) still evoked repetitive Ca^{2+} oscillations on an elevated baseline value while a low concentration of ATP (EC_{25}) evoked a rapid rise in Ca^{2+} followed by a decline back to resting values. This observation suggests that the distinctive different features of the Ca^{2+} signals evoked by each agonist were linked to the agonist rather than the cell.

Discussion

A major challenge faced by the endothelium is the need to process an enormous quantity of information held in the complex chemical environment to which the vascular system is exposed. From this information decisions on physiological outputs are made. The endothelium uses a multitude of receptors to continuously monitor vanishingly small changes in the concentration of extracellular signals (*2-5, 42*) that each provides cues to the ever-changing physiological state. Extracellular signals must be accurately detected and correctly relayed via intracellular Ca^{2+} signals so that information is not lost. Precisely how the endothelium processes the entire chemical composition to which it is exposed and transduces multiple extracellular signals, to specific cell activities is not fully understood. We have shown the endothelium uses spatially-structured arrangements of cells that extract small separate components of the overall information content. These components evoke distinctive Ca^{2+} and nitric oxide signals in specific clusters of cells. The Ca^{2+} signals are shared among cells. When more than one stimulus is present, computations are carried out on the input signals to generate new signals that are a composite of each input signal. The endothelium thus detects signals in a noisy environment by using cells that are not concerned with all possible available information but with only a small part of the overall content. These cells then collaborate with network partners in the distribution and integration of information.

The endothelium has a very large functional repertoire and controls virtually every cardiovascular function. Dysfunction of the endothelium underlies almost all cardiovascular disease. The short range network properties may determine the endothelium's sensing abilities and the effectiveness of information transfer. Despite the diverse functional activities of the endothelium, the anatomy and connectivity of the cells and network are largely fixed (each cell has 6 neighbors). The question of how a large functional signaling repertoire arises from a fixed anatomy and connectivity using a single communication signal (Ca^{2+}) both within and between cells is unresolved. Most studies on the endothelium provide information derived from large ensemble measurements in intact arteries or cultured cell models in which the behavior of the population is assumed to be uniform. When communication between cells is believed to occur, information arriving at one cell is thought to be conveyed to neighboring cells (e.g. other endothelial cells) without changing the information content much like signaling in a cable (*11,*

12). We developed an approach that provides an independent readout of hundreds of individual endothelial cells in intact arteries. The findings show there is divergence between structural and functional networks. While the endothelium has a defined, fixed, network architecture, responses to different extracellular signals are organized into separate local clusters or interactions of that network to ensure efficient message detection and for multiple simultaneous stimuli to be accommodated.

Our results show the response throughout the endothelium was not uniform and various regions selectively responded to different activators. In those regions, endothelial cells that activate to an agonist were found to be significantly more closely spaced (clustered) than expected if the agonist response was randomly distributed across cells. Different agonists activated different clusters of cells in separate regions or the endothelium. The clustering of cells with responsiveness to particular agonists may offer several advantages. Clustering may provide a co-incidence detection system to help improve signal detection (*8*). It is also tempting to speculate that clustering may allow the uptake and breakdown mechanisms for diffusible messengers (e.g. nitric oxide, prostaglandin) to be overwhelmed providing increased spillover of signals. Clustering may limit the interference from neighboring cells that are responding to a different stimulus. i.e. a single cell responding in isolation may easily be influenced by neighboring cells and have its signal overridden. A cluster performing the same task may be much harder to override. The mechanisms giving rise to the organization of cells into clusters are not yet clear but perhaps self-replication occurs during development or there is feedback control of function and receptor expression based on location or a result of a self-organization process at the cellular level.

In other studies various receptors have been reported to be heterogeneously distributed in the endothelium (*43*). The distribution of angiotensin II immunostaining is irregular in neighboring endothelial cells of femoral mesenteric artery (*44*). ACh-evoked Ca^{2+} responses are larger at branches in rat thoracic aorta than that of nearby non-branch regions (*38*). The reverse was true of histamine (*38*). The sensitivity to histamine and ACh was not distributed evenly among neighboring cells but arranged in 'belts' of high sensitivity that varied by ~100 fold along the flow lines (*38*). In studies of murine thoracic aorta endothelial cells, while most cells (82%) responded to ATP, large fractions of cells did not respond to ACh, bradykinin or substance P

(*45*). A mosaic pattern of micro-domains of VWF-positive and -negative endothelial cells occur in the capillaries of many vascular beds and in the aorta (*6, 44, 46*). Our results also show there is heterogeneity in the distribution of receptors (M3 and P2Y2) which offers and explanation for the heterogeneous responses. Single-cell profiling of primary endothelial cells revealed surprisingly high level of heterogeneity and patterning of G-protein coupled receptor expression in subpopulations of cells (*47*). While appreciated to exist, the physiological significance of the various receptor distributions and sensitivities and has not been understood. The heterogeneity in the distribution of receptors and clustering of sensing cells may be central to the function of the elaborate sensing system operating in the endothelium.

Many (*13-16, 29*) though not all (*20*) extracellular activators are transduced to changes in intracellular Ca^{2+} concentration to evoke specific cell activities. An unresolved question in Ca^{2+} signaling is how this single ion can selectively control virtually all cellular processes. Our data shows that Ca^{2+} signals evoked by low but equivalent (EC_{25}) concentrations of CCh and ATP in separate cells are distinctive. CCh evokes a small persistent rise in Ca^{2+} while ATP evokes an initial Ca^{2+} spike followed by a decline to basal values i.e. there is an input/output relationship between agonist and signal that is temporally-distinctive. When the agonists are applied separately at moderate concentrations (EC_{25}), most cells are sensitive to only one agonist (*unimodal* cells). However, some cells are sensitive to both (*multimodal* cells). Importantly, when the agonists are added separately, multimodal cells generates distinctive signals to each agonist. This observation suggests that the distinctive signals evoked by each agonist are a feature of the agonist acting on the cells rather than the cell itself.

When both agonists are present, a new signal output is generated that is distinct from each of the signals generated when the agonists are present separately. The generation of a new signal suggests that cells perform computations by combining information from each source to produce a new output. At least two mechanisms may give rise to the new distinctive signal. First, some cells (multimodal) possess receptors for both activators so a summation/averaging of activation of individual responses within these occurred. Alternatively, unimodal cells may be directly activated by only one agonist, and receive signals from another cell that is receptive to a different agonist. To test for the possibility that cells also received signals from other cells we examined signals in (the few) cells responded to neither the EC_{25} or EC_{75} of one agonist. Importantly, in

those cells that did not respond to one agonist (even at the EC_{75}) there was nonetheless modification of the signals to the other agonist when both were present at the EC_{25}. It seems likely that cells received signals (Ca^{2+} or IP_3) from neighboring cells to modify responses when both agonists were present.

Taken together these results suggest that different stimuli evoke distinctive signals in endothelial cell, that the input/output relationship for a given cell and agonist is not fixed and that cells act as computational elements when more than one signal is present. The precise nature of the computation is not clear but it appears that it is not a simple summation or averaging of each separate signal. In the case of the steady-state response, the computation appears to be non-linear and expansive in that the combined response exceeds linear summation of each input. The computation is a feature emerging from the collective dynamics of the endothelial network and provides a mechanism for the endothelium to interactively monitor external environments via sensing that is distributed on across separate cells. This arrangement may give rise to the diverse function in the endothelium arising from a fixed network structure that communicates using a single signaling molecule (Ca^{2+}).

The cardiovascular system undergoes continuous bombardment from a multitude of chemical instructions providing information on physiological status. Most signals are generated to evoke the continuous routine but small adjustments to cardiovascular function. As a result, many of the signals are of a very small magnitude and sit on a baseline concentration that is noisy and close in value to the normal peak increase (*2-5*). The normal daily concentration changes of circulating hormomes, such as parathyroid hormone, epinephrine, angiotensin II or leptin, is vanishing small and vary from a resting value of a few tens of *picomolar* to a peak increase in the low hundreds of *picomolar* (*2-5, 42*). The endothelium acts as the interface for the information and must detect the signals and decode an enormous quantity of data held in multiple signals to direct resources to the most behaviorally-relevant cardiovascular activity. The endothelium must also quickly redirect resources when faced with rapid physiological changes involving much higher local concentration changes such as those occurring during a bleeding event. The mechanisms by which the endothelium is capable of merging multiple agonist of varying concentration magnitudes are unknown. The data in the present study suggests that the processing of multiple chemical instructions is not achieved by each cell sensing every instruction but from the separate

activity of a collective of endothelial cells. Various endothelial cells encode only certain aspects of the overall information content. Communication of information among connected cells allows the endothelium to merge information and provide a more comprehensive “picture” of physiological status. Together, the observations suggest sensing and control is distributed among a number of endothelial cells and that spatial-structuring of sensory cells and temporal-encoding of signals is fundamental to endothelial signal detection. As a collective the endothelium can efficiently process multiple instructions and act as a sensory system that has substantially greater computational power than the capabilities of any single cell.

Materials and Methods

Animals

All animal care and experimental procedures were carried out with the approval of the University of Strathclyde Animal Welfare and Ethical Review Board (Schedule 1 procedure; Animals (Scientific Procedures) Act 1986, UK), under UK Home Office regulations. All experiments utilized freshly isolated rat carotid arteries obtained from male Sprague–Dawley rats (10–12 weeks old; 250–350 g) killed by intraperitoneal overdose of pentobarbital sodium (200 mg kg^{-1}, Pentaject, Merial Animal Health Ltd, UK) CO_2 overdose.

En face artery preparation

Endothelial Ca^{2+} signaling was imaged in *en face* carotid artery preparations (*31*). Arteries were cut open along their longitudinal axis, using microscissors, and pinned out on a Sylgard block, with the lumen side upward. Endothelial cells were incubated with a physiological saline solution (PSS) containing the fluorescent Ca^{2+} indicator, Cal-520 acetoxymethyl ester (Cal-520/AM) (5μM), 0.02% Pluronic F-127 and 0.35% DMSO for 30 min at 37°C. After incubation the arteries were gently washed with PSS at room temperature and allowed to equilibrate for 30 minutes. The Sylgard block containing the artery was placed in a custom bath chamber that was fixed to the stage of an inverted fluorescence microscope (TI-E; Nikon, UK). The bottom of the bath chamber was a 0-grade thickness microscope coverslip. Two 200 μm pins were used to raise the Sylgard block from the coverslip so that the endothelium did not contact the glass coverslip and permitting solutions to be flowed through the chamber. Laminar flow was provided by a syringe pump that was connected to the chamber via silicone tubing. Solutions were flowed into the bath at a rate of 1.5 ml/min.

Cal-520/AM was excited with 488 nm excitation light provided by a monochromator (Photon Technology International/Horiba UK, Ltd., UK) and imaged using a back-illuminated electron-multiplying charge coupled device (EMCCD) camera (iXon3; Andor, Belfast, UK; 13 μm pixel size) through a 40X (oil immersion; numerical aperture 1.3; Nikon S Fluor) objective lens (*48, 49*). Fluorescence emission was recorded at 10 Hz. Fluorescence illumination was controlled and images (16-bit depth) captured using WinFluor (WinFluor, University of Strathclyde, Glasgow, UK). Following each pharmacological activation, the preparation was washed with PSS for 5

minutes and then allowed to rest for a further 5 minutes to ensure a stable baseline was established before subsequent drug applications.

Cholinergic and Purinergic Ca^{2+} Signaling

Endothelial Ca^{2+} signaling was examined in response to muscarinic and purinergic agonists. Full non-cumulative concentration responses were obtained in each *en face* preparations by applying each of the agonists at various concentrations (CCh from 1 nM to 30 μM; ATP 100 nM to 1mM). Only one concentration-response curve was generated per carotid artery preparation.

In experiments designed to analyze the first responding cells (at EC_{25} and EC_{75} concentrations) the agonists were sequentially applied to the same artery preparation and recordings were made from the same field of endothelium for the EC_{25} and EC_{75} concentrations for both agonists. The EC_{25} and EC_{75} values were obtained from concentration-response curves showing the 'percentage of active cells'. Both agonists were then applied simultaneously, at the EC_{25} concentration, to the same artery to determine any interaction between the two agonists in the cells activated.

In experiments designed to determine the receptor subtype involved in CCh evoked Ca^{2+} signaling a selective M3 antagonist 4-DAMP (100 nM) was used. To determine whether metabotropic or ionotropic receptors were involved in ATP evoked Ca^{2+} signaling, ATP was applied to the endothelium in Ca^{2+}-Free PSS. Specific P2Y1 receptor antagonist (MRS2179; 10 μM) and P2Y2 receptor antagonist (ARC118925; 1 uM) were used to discern the metabotropic receptor subtype involved in ATP evoked Ca^{2+} signaling.

Automated Ca^{2+} signal analysis

Due to the large number of cells imaged, manual analysis of each individual cell was impractical. Therefore, automated analysis software (WAVE; Whole-cell AVErage) was used to extract Ca^{2+} signals from every cell in the field-of-view (Wilson *et al*., 2016). In brief, (1) all cells within the field-of-view are identified and a region of interest (ROI) that encompasses the cell area is created; (2) the Ca^{2+} signals from each ROI are extracted as time-dependent fluorescence intensities (3) each Ca^{2+} signal is normalized to its corresponding baseline; (4) Ca^{2+} signaling metrics, such as peak amplitudes and oscillation frequency, are rapidly and objectively

determined for all cells (ROIs); and (5) Ca^{2+} signals and summary data are presented in pictorial form. The Ca^{2+} signal from precisely the same cell can be matched across different experiments.

ROI Generation

Intensity thresholding of the raw image does not yield accurate cellular ROIs due to the high density of endothelial cells in intact arteries. Instead, average intensity projections were sharpened using an unsharp masking macro written in ImagePro (Schindelin *et al*., 2012). After sharpening, individual cellular ROIs were obtained by intensity thresholding (in ImagePro) and manually splitting any ROI that overlapped two (or more) cells. To enable a comparison (i.e. pairing) of the response of individual cells after various treatments during an experiment, cellular ROIs were generated from a single control dataset were applied to all responses obtained in that single experiment. Where slight tissue movement occurred between acquisitions, ROI's were aligned across individual datasets using an automated alignment plug-in in FIJI (Schindelin *et al*., 2012). Each ROI (Cell) was assigned an individual number (Cell #) for identification throughout and enable a direct comparison of the same cell in response to different treatments.

Automated whole-cell Ca^{2+} signal extraction

Ca^{2+} signals were calculated for each individual cell from the Cal-520/AM fluorescence intensity within each ROI. Each signal was expressed as baseline-corrected fluorescence intensity (F/F_0), where F is fluorescence at time, t, and F_0 is basal fluorescence intensity. F_0 was determined for each individual ROI by averaging a 100-frame (10 second) baseline period at the start of each recording. F/F_0 traces were smoothed using 11-point (1.1 s), third-order polynomial Savitzky–Golay filter.

Automated whole-cell Ca^{2+} signal analysis

Endothelial Ca^{2+} signals exhibit oscillatory behavior. The occurrence of these oscillations was identified automatically using the discrete (first) derivative ($d(F/F_0)/dt$) of the Ca^{2+} signal (F/F_0). Discrete derivate signals were calculated by convolving F/F_0 traces with the first derivative of a Gaussian kernel in the programming language, Python (*8, 50*). An increase in F/F_0 corresponds to a positive deflection in the discrete derivative and a decrease in F/F_0 corresponds to a negative deflection in the discrete derivative. At the peak of an F/F_0 Ca^{2+} spike the derivative changes

sign from positive to negative. A 'zero-crossing detector' was used on the discrete derivative to identify the time at which peaks occurred in the F/F_0 data i.e. when the sign of the rate changed from positive to negative and the rate of change is zero. The zero-crossing detector provided a list of times of 'zero-crossing' – i.e. the times at which a peak occurs in the data. Therefore, the zero-crossing detector enabled the times of all peaks, with a magnitude greater than 10-times the standard deviation of baseline noise (considered to be the threshold), in the derivate signal to be extracted. Those times were then used to extract conventional measurements (e.g. amplitude) from the corresponding F/F_0 data. The detection of a peak from the discrete derivative trace (above threshold) was used to determine if a cell responded. If a peak was detected in a cell, the cell was defined as being 'active'. Oscillatory Ca^{2+} signals evoked by the agonists were measured in terms of peak amplitude of the initial Ca^{2+} rise, the response averaged over 60-seconds following this peak, and percentage of the total number of cells which responded. The times of occurrence of the first peak in each Ca^{2+} response were used to generate latency profiles of cellular Ca^{2+} responses. These latency profiles are presented as histograms with time, $t = 0$, corresponding to the time of the first detected peak.

Ca^{2+} responses were recorded over a five-minute period. This allowed for the recording of basal Ca^{2+} activity (no agonist; ~1-2 minutes) and the response to stimuli (~3-4 minutes)

Cell Clustering and Neighbor Analysis

In order to examine the spatial relationship of cell responses, a robust means to define spatial relationships between cells was required. For this purpose we used a modification of a Voronoi tessellation (*51, 52*). Briefly, the center coordinates of each biological cell's nucleus forms a vertex in a Voronoi tessellation. The tellsellation partitions the image space into a series of Voronoi cells. Each Voronoi cell contains all points closer to its vertex than to any other vertex. Each edge in the Voronoi diagram separates two Voronoi cells and represents all points in space equidistant to the coordinates of the two nuclei that define the two Voronoi cells, and that are closer to those nuclei than to any other. We use each edge in the tessellation to define the corresponding biological cells to be "Voronoi neighbors". Voronoi tessellation and subsequent analysis was carried out in the Python language version 2.7.11 using the scipy (*53*) and numpy (*54*) libraries, versions 0.17.0 and 1.10.4 respectively.

Nitric oxide imaging and analysis

Arteries were pinned flat in a custom made bath chamber and pre-loaded with Cal-520 as described above to identify endothelial cell positions. To measure nitric oxide production arteries were then incubated in HANKS buffer solution containing DAR-4 AM, a cell permeable nitric oxide reporting fluorophore (100 μM DAR-4M AM, 0.02% Pluronic F-127 and 100 μM L-arginine) for 30 minutes at room temperature. After incubation arteries were gently washed with HANKS buffer and allowed to equilibrate for 30 minutes. Laminar flow was provided by a syringe pump that was connected to the chamber via silicone tubing. Solutions were flowed into the bath at a rate of 1.5 ml/min. DAR-4M AM was excited using 550 nm wide-field epifluorescence illumination provided by a monochomator (Photon Technology International/Horiba UK, Ltd., Stanmore, United Kingdom) and visualized using a back-illuminated electron-multiplying charge coupled device (EMCCD) camera (iXon Life 888; Andor, Belfast, UK; 13 μm pixel size) through a 60X (water immersion; numerical aperture 1.0; Nikon S Fluor) objective lens. Fluorescence emission was recorded at 10 Hz. Fluorescence illumination was controlled and images (16-bit depth) captured using μManager software (Edelstein et al. 2010). Following each pharmacological activation (with CCh or ATP), the preparation was washed with HANKS buffer for 10 minutes and then allowed to rest for a further 10 minutes to ensure a stable baseline was established before subsequent drug applications.

Automated analysis was carried out as described above to calculate the nitric oxide production for each individual cell. ROI's were generated using the Cal-520 loading, imaged at 488 nm. Nitric oxide production was recorded over a five-minute period. This allowed for the recording of basal nitric oxide activity (no agonist; ~1-2 minutes) and the response to stimuli (~3-4 minutes).

Endothelial Immunocytochemistry

Arteries were pinned to a 6 well plate containing Sylgard and fixed in 4% Paraformaldehyde for 20 minutes at room temperature. Arteries were washed 3 times in 100 μM glycine solution followed by 3 washes with PBS, permeabilzed with 0.2% Triton-X100 in PBS for 10 minutes and washed again 3 times with PBS. Arteries were then incubated in Antibody Buffer solution in PBS for 1 hour at room temperature then washed 3 times with Antibody wash solution

containing 5% BSA. The arteries then were incubated with a rabbit anti-P2Y2 receptor antibody (1:100, sc-20124, Santa Cruz, Dallas, TX, USA) and CD31 (1:200, AF3628, R&D Systems,) in PBS containing 1% BSA and 2% Donkey Serum for 12 hours at 4°C. Arteries were washed with Antibody wash solution containing 5% BSA 3 times followed by incubation with Alexa Fluor 488 donkey anti-rabbit antibody (Invitrogen, Carlsbad, CA, USA) and Alexa Fluor 568 donkey anti-goat antibody (Invitrogen, Carlsbad, CA, USA) in Antibody Buffer Solution for 1 hour at room temperature. The P2Y2 Receptor Antibody was excited using 488 nm and CD31 Antibody was excited using 568 nm wide-field epifluorescence illumination provided by a monochomator (Photon Technology International/Horiba UK, Ltd., Stanmore, United Kingdom) and visualized using a back-illuminated electron-multiplying charge coupled device (EMCCD) camera (iXon Life 888; Andor, Belfast, UK; 13 μm pixel size) through a 60X (water immersion; numerical aperture 1.0; Nikon S Fluor) objective lens. Fluorescence emission was recorded at 10 Hz. Fluorescence illumination was controlled and images (16-bit depth) captured using ImageJ (National Institutes of Health, Bethesda, MD, USA). Negative controls were performed in the absence of primary antibody.

Fluorescent Ligand Binding in Intact Endothelium

To visualize P2Y2 Receptors and M3 Receptor distribution, P2Y2-antibody stained arteries were loaded with a Fluorescent Muscarinic M3 receptor Antagonist (M3-633-AN, 100 nM; Sigma-Aldrich) for 20 minutes at room temperature. The Fluorescent Muscarinic M3 receptor Antagonist was excited at 633 nm and visualized as described above. Negative controls were performed in the presence of the selective M3 receptor antagonist 4-DAMP (10 μM, 20 minute incubation before Fluorescent Muscarinic M3 receptor Antagonist loading). P2Y2, M3 and PECAM visualization was carried out in precisely the same area of endothelium by changing the excitation wavelength.

Cell boundaries were identified using PECAM-1 fluorescence. From these boundaries ROI's were manually extracted to identify individual endothelial cells. The area of M3, P2Y2 expression and the extent of co-localization (M3 and P2Y2 overlap) were then determined within each cell (using the ROIs) and from the full field of view using ImageJ.

P2Y2 Receptor Antibody Validation

Specificity of the antibody for P2Y2 receptors (sc-20124, 1:100, Santa Cruz, Dallas, TX, USA) was confirmed in experiments carried out in cell lines that either (1) completely lack P2Y receptors or (2) express only P2Y2 receptors (Supplementary Fig S7). 1321N1 cells (ECACC Cat# 86030402, RRID:CVCL_0110) are a human astrocytoma cell line that does not endogenously express any of the eight P2Y receptor subtypes or respond to the naturally-occurring nucleotide agonist (*41*) and were used as a negative control for the antibody. 1321N1 cells stably expressing recombinant human hP2Y2 receptors (1321N1-hP2Y2)(*40*) were used as a positive control (Supplementary Fig S7).

Wild-type 1321N1 cells and 1321N1 cells stably expressing recombinant human $hP2Y_2$ receptors (1321N1-hP2Y2) (*40*) were maintained in 5% CO_2, 95% O_2 in a humidified incubator at 37°C, in Dulbecco's Modified Eagles Media (Life Technologies, Paisley, UK, catalogue number 21969-035), supplemented with 10% foetal calf serum, 1% non-essential amino acids, 1% penicillin (10,000 units/ml) and streptomycin (10 mg/ml).

The wild-type 1321N1 cells and 1321N1 cells stably expressing recombinant human hP2Y2 receptors (1321N1-hP2Y2) were fixed in 4% Paraformaldehyde for 20 minutes at room temperature and washed 3 times in 100 μM glycine solution followed by 3 washes with PBS. Cells were then incubated in Antibody Buffer solution in PBS for 1 hour at room temperature then washed 3 times with Antibody wash solution containing 5% BSA. The cells were then incubated with a rabbit anti-P2Y2 receptor antibody (1:100, sc-20124, Santa Cruz, Dallas, TX, USA) in PBS containing 1% BSA and 2% Donkey Serum for 2 hours at 4°C. Cells were washed with Antibody wash solution containing 5% BSA 3 times followed by incubation with Alexa Fluor 488 donkey anti-rabbit antibody (Invitrogen, Carlsbad, CA, USA) in Antibody Buffer Solution for 1 hour at room temperature. The P2Y2 Receptor Antibody was excited using 488 nm wide-field epifluorescence illumination provided by a LED (CoolLED pE-300^{ultra}, CoolLED Ltd, Andover, UK) and visualized using a back-illuminated electron-multiplying charge coupled device (EMCCD) camera (iXon Life 888; Andor, Belfast, UK; 13 μm pixel size) through a 40X (oil immersion; numerical aperture 1.3; Nikon S Fluor) objective lens. Fluorescence emission was recorded at 10 Hz. Fluorescence illumination was controlled and images (16-bit depth) captured using ImageJ (National Institutes of Health, Bethesda, MD, USA). Cells were incubated

in PBS containing 0.5mg/ml DAPI to visualize the nucleus of endothelial cells. DAPI was excited at 365 nm and visualized as described above.

P2Y2 receptor distribution was quantified as fluorescence intensity levels. Since there was an almost complete absence of staining in 1321N1 cells (which lack P2Y receptors) full field fluorescence was measured. Cell nuclei counts using DAPI staining ensured comparable cell number in wild-type and P2Y2 expressing cells.

Pressure Myography

The left and right common carotid arteries were exposed by sharp dissection and both arteries were extracted and placed in HANKS buffer solution. Under a stereomicroscope arteries were cleaned of connective tissue and visually checked for the presence of side branches. Arteries without side branches were mounted onto two blunted, sterile 25G x 5/8" BD Microlance Needles (0.51mm Outer Diameter) using silk suture thread, in a self-heated single vessel chamber (CH-1-AU-SH, Living Systems Instrumentation, Albans City, VT, USA). Arteries were gently heated to 37°C and allowed to equilibrate for 30 minutes. The proximal end of each BD Microlance Needle was connected to a separate syringe containing HANKS buffer solution. The height of two syringes was adjusted to alter the transmural pressure of the arteries. The pressure was increased in 10 mmHg increments with 10 minute equilibration allowed before subsequent increases in pressure. When a final pressure of 110 mmHg was attained arteries were allowed to equilibrate for 30 minutes. During equilibration arteries were tested for leaks (which may indicate branches in the vessel wall or insufficiently tied sutures) by stopping the flow of solution from the syringes to the arteries by switching the valves connecting the syringes to the BD Microlance Needles. This allowed the pressure within the arteries to remain constant. Arteries that showed a reduction in pressure were discarded. HANKS buffer was circulated in the chamber that contained the arteries at 10 ml/min using a peristaltic pump from a reservoir (heated to 37°C).

To determine the vasorelaxant effects of CCh and ATP, arteries were first contracted using phenylephrine (100 μM), applied to the outside of the artery by adding the agonist to the reservoir and allowing it to circulate. Arteries were then allowed to equilibrate to ensure a stable contraction was achieved before subsequent drug applications. CCh or ATP were applied to the

arteries intraluminally. To do this, the height of one syringe was adjusted to allow gravitational flow (0.5 ml/min) of solution through the lumen of the artery. CCh (100 μM) was applied by adding the drug to the higher of the two syringes that perfused the artery lumen. Arteries were then allowed to equilibrate for 20 minutes (10 minutes for the drug to reach the lumen; 10 minutes of activation). Following activation, the solution in the syringe was removed and replaced with HANKS buffer. Arteries were washed intraluminally with HANKS buffer until arteries returned to a contracted state. ATP (100 μM) was subsequently applied to the same artery, as described above.

In experiments designed to determine endothelial Ca^{2+} dependence of CCh- and ATP-mediated vasodilation, BAPTA-AM (30 μM), a cell-permeable selective Ca^{2+}- chelator was applied intraluminally as described above. Preconstricted arteries were allowed to equilibrate in BAPTA-AM for 30 minutes prior to the addition of CCh (100 μM) and ATP (100 μM). The effects of the Ca^{2+} chelator (BAPTA) on CCh and ATP evoked relaxation was compared to internal controls with each vasodilator carried that were out in the same artery.

Artery images were recorded using a CMOS camera (DCC1545; ThorLabs Inc. Newton, New Jersey, USA; 5.2 μm pixel size) through a 2.5X (air; numerical aperture 0.06; Zeiss A-Plan) objective lens. Images (8-bit depth) were captured using μManager software (*55*).

Drugs and solutions

Cal-520/AM was obtained from Abcam (Cambridge, MA, USA). Pluronic F-127 was obtained from Invitrogen (Carlsbad, CA, USA). AR-C 118925XX and MRS 2179 were obtained from Tocris (Abingdon, UK). P2Y2 Antibody (H-70) was obtain from Santa Cruz (Dallas, TX, USA). CD31/PECAM-1 antibody was obtained from R&D Systems (Minneapolis, MN, USA). All other drugs and chemicals were obtained from Sigma (St Louis, MO, USA). The PSS consisted of (mM): 145 NaCl, 4.7 KCl, 2.0 MOPS, 1.2 NaH_2PO_4, 5.0 glucose, 0.02 EDTA, 1.17 $MgCl_2$, 2.0 $CaCl_2$, adjusted to pH 7.4 with NaOH. The Ca^{2+}-Free PSS consisted of (mM): 145 NaCl, 4.7 KCl, 2.0 MOPS, 1.2 NaH_2PO_4, 5.0 glucose, 0.02 EDTA, 1.0 EGTA, 2.34 $MgCl_2$, adjusted to pH 7.4 with NaOH. HANKS buffer consisted of (mM): 125 NaCl, 5.4 KCl, 4.2 $NaHCO_3$, 0.4 KH_2PO_4, 0.3 NaH_2PO_4, 10 HEPES 10.0 glucose, 1.17 $MgCl_2$, 2.0 $CaCl_2$, adjusted to pH 7.4 with NaOH. Antibody Buffer solution consisted of: 0.05% Triton-X100, 0.02% Sodium Azide, 5%

SSC (20X). Antibody wash solution consisted of: 5% SSC (20X), 0.05% Triton-X100, 5% BSA. All solutions were freshly prepared daily.

Statistics

The data are presented as mean ± SEM values; *n* refers to *n* arteries obtained from *n* different animals (biological replicates). For comparison of two groups, a Student's t test (paired data) or unpaired t-test (unpaired data) was performed. All statistical analyses were performed using GraphPad Prism, version 6.0 (GraphPad Software, La Jolla, CA, USA). $p < 0.05$ was considered statistically significant.

Supplementary Materials

Supplementary Fig S1 CCh evoked Ca^{2+} signals in the endothelium.

Supplementary Fig S2 Flow-induced endothelial Ca^{2+} signaling

Supplementary Fig S3 Endothelial Ca^{2+}-dependence of endothelial-evoked dilation

Supplementary Fig S4 Concentration-dependence of the CCh-evoked endothelial Ca^{2+} response.

Supplementary Fig S5 Concentration-dependence of the ATP-evoked endothelial Ca^{2+} response.

Supplementary Fig S6 The pattern of cell activation is unaltered by sequence of agonist addition

Supplementary Fig S7 Specificity of the P2Y2 receptor antibody for P2Y2 receptors

Supplementary Fig S8 Heterogeneity in nitric oxide production

Supplementary Movie S1 Regional Ca^{2+} signals evoked by CCh (100 nM). Video x10 real time

Supplementary Movie S2 Spatial separate cell clusters activated by the EC25 concentrations of CCh (green) and ATP (red). Video x10 real time.

REFERENCES

1. H. F. Galley, N. R. Webster, Physiology of the endothelium. *Br J Anaesth* **93**, 105-113 (2004).
2. J. Licinio, A. B. Negrao, C. Mantzoros, V. Kaklamani, M. L. Wong, P. B. Bongiorno, A. Mulla, L. Cearnal, J. D. Veldhuis, J. S. Flier, S. M. McCann, P. W. Gold, Synchronicity of frequently sampled, 24-h concentrations of circulating leptin, luteinizing hormone, and estradiol in healthy women. *Proc Natl Acad Sci U S A* **95**, 2541-2546 (1998).
3. N. Kitamura, C. Shigeno, K. Shiomi, K. C. Lee, S. Ohta, T. Sone, S. Katsushima, E. Tadamura, T. Kousaka, I. Yamamoto, S. Dokoh, J. Konishi, Episodic Fluctuation in Serum Intact Parathyroid-Hormone Concentration in Men. *J Clin Endocr Metab* **70**, 252-263 (1990).
4. C. Schofl, C. Becker, K. Prank, A. Von Zur Muhlen, G. Brabant, Twenty-four-hour rhythms of plasma catecholamines and their relation to cardiovascular parameters in healthy young men. *Eur J Endocrinol* **137**, 675-683 (1997).
5. C. Dodt, U. Breckling, I. Derad, H. L. Fehm, J. Born, Plasma epinephrine and norepinephrine concentrations of healthy humans associated with nighttime sleep and morning arousal. *Hypertension* **30**, 71-76 (1997).
6. L. Yuan, G. C. Chan, D. Beeler, L. Janes, K. C. Spokes, H. Dharaneeswaran, A. Mojiri, W. J. Adams, T. Sciuto, G. Garcia-Cardena, G. Molema, P. M. Kang, N. Jahroudi, P. A. Marsden, A. Dvorak, E. R. Regan, W. C. Aird, A role of stochastic phenotype switching in generating mosaic endothelial cell heterogeneity. *Nature communications* **7**, 10160 (2016).
7. W. C. Aird, Endothelial cell heterogeneity. *Cold Spring Harbor perspectives in medicine* **2**, a006429 (2012).
8. C. Wilson, Saunter, C.D., Girkin, J.M. & McCarron, J.G., Clusters of specialized detector cells provide sensitive and high fidelity receptor signaling in intact endothelium. *Faseb J.* **30**, 2000-2013 (2016).
9. J. G. McCarron, M. D. Lee, C. Wilson, The Endothelium Solves Problems That Endothelial Cells Do Not Know Exist. *Trends Pharmacol Sci* **38**, 322-338 (2017).
10. P. Paszek, S. Ryan, L. Ashall, K. Sillitoe, C. V. Harper, D. G. Spiller, D. A. Rand, M. R. White, Population robustness arising from cellular heterogeneity. *Proc Natl Acad Sci U S A* **107**, 11644-11649 (2010).
11. T. Duza, I. H. Sarelius, Localized transient increases in endothelial cell Ca2+ in arterioles in situ: implications for coordination of vascular function. *Am J Physiol Heart Circ Physiol* **286**, H2322-2331 (2004).
12. Y. N. Tallini, J. F. Brekke, B. Shui, R. Doran, S. M. Hwang, J. Nakai, G. Salama, S. S. Segal, M. I. Kotlikoff, Propagated endothelial Ca^{2+} waves and arteriolar dilation in vivo: measurements in Cx40BAC GCaMP2 transgenic mice. *Circ Res* **101**, 1300-1309 (2007).
13. P. Bagher, T. Beleznai, Y. Kansui, R. Mitchell, C. J. Garland, K. A. Dora, Low intravascular pressure activates endothelial cell TRPV4 channels, local Ca^{2+} events, and IKCa channels, reducing arteriolar tone. *Proc Natl Acad Sci U S A* **109**, 18174-18179 (2012).
14. L. Borisova, S. Wray, D. A. Eisner, T. Burdyga, How structure, Ca signals, and cellular communications underlie function in precapillary arterioles. *Circ Res* **105**, 803-810 (2009).

15. A. Luckhoff, U. Pohl, A. Mulsch, R. Busse, Differential role of extra- and intracellular calcium in the release of EDRF and prostacyclin from cultured endothelial cells. *Br J Pharmacol* **95**, 189-196 (1988).
16. C. Prendergast, J. Quayle, T. Burdyga, S. Wray, Atherosclerosis differentially affects calcium signalling in endothelial cells from aortic arch and thoracic aorta in Apolipoprotein E knockout mice. *Physiological reports* **2**, (2014).
17. S. K. Sonkusare, A. D. Bonev, J. Ledoux, W. Liedtke, M. I. Kotlikoff, T. J. Heppner, D. C. Hill-Eubanks, M. T. Nelson, Elementary Ca^{2+} signals through endothelial TRPV4 channels regulate vascular function. *Science* **336**, 597-601 (2012).
18. J. Ledoux, M. S. Taylor, A. D. Bonev, R. M. Hannah, V. Solodushko, B. Shui, Y. Tallini, M. I. Kotlikoff, M. T. Nelson, Functional architecture of inositol 1,4,5-trisphosphate signaling in restricted spaces of myoendothelial projections. *Proc Natl Acad Sci U S A* **105**, 9627-9632 (2008).
19. T. A. Longden, F. Dabertrand, M. Koide, A. L. Gonzales, N. R. Tykocki, J. E. Brayden, D. Hill-Eubanks, M. T. Nelson, Capillary K+-sensing initiates retrograde hyperpolarization to increase local cerebral blood flow. *Nature Neuroscience* **20**, 717-+ (2017).
20. J. A. Stolwijk, X. Zhang, M. Gueguinou, W. Zhang, K. Matrougui, C. Renken, M. Trebak, Calcium Signaling Is Dispensable for Receptor Regulation of Endothelial Barrier Function. *J Biol Chem* **291**, 22894-22912 (2016).
21. M. Feletou, in *The Endothelium: Part 1: Multiple Functions of the Endothelial Cells-Focus on Endothelium-Derived Vasoactive Mediators*. (San Rafael (CA), 2011).
22. D. E. Clapham, Calcium signaling. *Cell* **131**, 1047-1058 (2007).
23. M. J. Berridge, P. Lipp, M. D. Bootman, The versatility and universality of calcium signalling. *Nat Rev Mol Cell Biol* **1**, 11-21 (2000).
24. J. G. McCarron, S. Chalmers, K. N. Bradley, D. Macmillan, T. C. Muir, Ca^{2+} microdomains in smooth muscle. *Cell Calcium* **40**, 461-493 (2006).
25. J. H. Jaggar, M. T. Nelson, Differential regulation of Ca^{2+} sparks and Ca^{2+} waves by UTP in rat cerebral artery smooth muscle cells. *Am J Physiol Cell Physiol* **279**, C1528-1539 (2000).
26. J. G. McCarron, Chalmers, S., MacMillan, D. & Olson, M.L, Agonist-evoked Ca^{2+} wave progression requires Ca^{2+} and IP_3. *Journal of Cell Physiology* **244**, 334-344 (2010).
27. L. Leybaert, M. J. Sanderson, Intercellular Ca^{2+} waves: mechanisms and function. *Physiol Rev* **92**, 1359-1392 (2012).
28. I. Parker, I. F. Smith, Recording single-channel activity of inositol trisphosphate receptors in intact cells with a microscope, not a patch clamp. *J Gen Physiol* **136**, 119-127 (2010).
29. M. Francis, J. R. Waldrup, X. Qian, V. Solodushko, J. Meriwether, M. S. Taylor, Functional Tuning of Intrinsic Endothelial Ca2+ Dynamics in Swine Coronary Arteries. *Circ Res* **118**, 1078-1090 (2016).
30. Q. Zou, S. W. Leung, P. M. Vanhoutte, Transient Receptor Potential Channel Opening Releases Endogenous Acetylcholine, which Contributes to Endothelium-Dependent Relaxation Induced by Mild Hypothermia in Spontaneously Hypertensive Rat but Not Wistar-Kyoto Rat Arteries. *J Pharmacol Exp Ther* **354**, 121-130 (2015).
31. C. Wilson, M. Lee, J. G. McCarron, Acetylcholine released by endothelial cells facilitates flow-mediated dilatation. *J Physiol* **594**, 7267–7307 (2016).

32. P. Bodin, G. Burnstock, Increased release of ATP from endothelial cells during acute inflammation. *Inflammation research : official journal of the European Histamine Research Society ... [et al.]* **47**, 351-354 (1998).
33. K. M. Meyers, H. Holmsen, C. L. Seachord, Comparative study of platelet dense granule constituents. *Am J Physiol* **243**, R454-461 (1982).
34. J. G. De Mey, P. M. Vanhoutte, Role of the intima in cholinergic and purinergic relaxation of isolated canine femoral arteries. *J Physiol* **316**, 347-355 (1981).
35. N. Tanaka, K. Kawasaki, N. Nejime, Y. Kubota, K. Takahashi, M. Hashimoto, M. Kunitomo, K. Shinozuka, P2Y receptor-mediated enhancement of permeation requires Ca2+ signalling in vascular endothelial cells. *Clin Exp Pharmacol Physiol* **30**, 649-652 (2003).
36. D. Gunduz, F. Hirche, F. V. Hartel, C. W. Rodewald, M. Schafer, G. Pfitzer, H. M. Piper, T. Noll, ATP antagonism of thrombin-induced endothelial barrier permeability. *Cardiovasc Res* **59**, 470-478 (2003).
37. W. C. Aird, Spatial and temporal dynamics of the endothelium. *Journal of thrombosis and haemostasis : JTH* **3**, 1392-1406 (2005).
38. T. Y. Huang, T. F. Chu, H. I. Chen, C. J. Jen, Heterogeneity of [Ca^{2+}]i signaling in intact rat aortic endothelium. *FASEB J* **14**, 797-804 (2000).
39. P. Kameritsch, K. Pogoda, A. Ritter, S. Munzing, U. Pohl, Gap junctional communication controls the overall endothelial calcium response to vasoactive agonists. *Cardiovasc Res* **93**, 508-515 (2012).
40. R. A. Nicholas, W. C. Watt, E. R. Lazarowski, Q. Li, K. Harden, Uridine nucleotide selectivity of three phospholipase C-activating P2 receptors: identification of a UDP-selective, a UTP-selective, and an ATP- and UTP-specific receptor. *Mol Pharmacol* **50**, 224-229 (1996).
41. M. P. Abbracchio, G. Burnstock, J. M. Boeynaems, E. A. Barnard, J. L. Boyer, C. Kennedy, G. E. Knight, M. Fumagalli, C. Gachet, K. A. Jacobson, G. A. Weisman, International Union of Pharmacology LVIII: update on the P2Y G protein-coupled nucleotide receptors: from molecular mechanisms and pathophysiology to therapy. *Pharmacological reviews* **58**, 281-341 (2006).
42. R. Kala, F. Fyhrquist, A. Eisalo, Diurnal variation of plasma angiotensin II in man. *Scandinavian journal of clinical and laboratory investigation* **31**, 363-365 (1973).
43. O. Cleaver, D. A. Melton, Endothelial signaling during development. *Nat Med* **9**, 661-668 (2003).
44. A. Tomlinson, H. Van Vlijmen, A. Loesch, G. Burnstock, An immunohistochemical study of endothelial cell heterogeneity in the rat: observations in "en face" Hautchen preparations. *Cell Tissue Res* **263**, 173-181 (1991).
45. I. Marie, J. L. Beny, Calcium imaging of murine thoracic aorta endothelium by confocal microscopy reveals inhomogeneous distribution of endothelial cells responding to vasodilator agents. *J Vasc Res* **39**, 260-267 (2002).
46. Y. A. Senis, M. Richardson, S. Tinlin, D. H. Maurice, A. R. Giles, Changes in the pattern of distribution of von Willebrand factor in rat aortic endothelial cells following thrombin generation in vivo. *British journal of haematology* **93**, 195-203 (1996).
47. H. Kaur, J. Carvalho, M. Looso, P. Singh, R. Chennupati, J. Preussner, S. Gunther, J. Albarran-Juarez, D. Tischner, S. Classen, S. Offermanns, N. Wettschureck, Single-cell

profiling reveals heterogeneity and functional patterning of GPCR expression in the vascular system. *Nature communications* **8**, (2017).
48. S. Chalmers, C. Saunter, C. Wilson, P. Coats, J. M. Girkin, J. G. McCarron, Mitochondrial motility and vascular smooth muscle proliferation. *Arterioscler Thromb Vasc Biol* **32**, 3000-3011 (2012).
49. M. L. Olson, S. Chalmers, J. G. McCarron, Mitochondrial Ca^{2+} uptake increases Ca^{2+} release from inositol 1,4,5-trisphosphate receptor clusters in smooth muscle cells. *J Biol Chem* **285**, 2040-2050 (2010).
50. C. Wilson, C. D. Saunter, J. M. Girkin, J. G. McCarron, Pressure-dependent regulation of Ca^{2+} signaling in the vascular endothelium. *J Physiol* **593**, 5231–5253 (2015).
51. S. Chalmers, C. D. Saunter, J. M. Girkin, J. G. McCarron, Flicker-assisted localization microscopy reveals altered mitochondrial architecture in hypertension. *Nature Scientific Reports* **30**, 2000-2013 (2015).
52. S. Chalmers, C. D. Saunter, J. M. Girkin, J. G. McCarron, Age decreases mitochondrial motility and increases mitochondrial size in vascular smooth muscle. *J Physiol* **594**, 4283-4295 (2016).
53. E. Jones, E. Oliphant, P. Peterson, et al., SciPy: Open Source Scientific Tools for Python *http://www.scipy.org/* (2001).
54. S. van der Walt, S. C. Colbert, G. Varoquaux, The NumPy Array: A Structure for Efficient Numerical Computation. *Comput Sci Eng* **13**, 22-30 (2011).
55. A. Edelstein, N. Amodaj, K. Hoover, R. Vale, N. Stuurman, Computer control of microscopes using microManager. *Current protocols in molecular biology / edited by Frederick M. Ausubel ... [et al.]* **Chapter 14**, Unit14 20 (2010).

Acknowledgments

This work was funded by the Wellcome Trust (202924/Z/16/Z) and the British Heart Foundation (PG/16/54/32230; PG16/82/32439),whose support is gratefully acknowledged. CW is supported by a Sir Henry Wellcome Postdoctoral Research Fellowship (204682/Z/16/Z).

Author Contributions

Conceptualization, JMcC, CW and ML; Methodology, ML, CW, CS, JG and JMcC; Investigation, ML, CK and CW; Writing – Original Draft, ML and JMcC; Writing – Review & Editing, JMcC, ML, CW, CS, CK, JG; Funding Acquisition, JMcC, CW, CS and JG; Resources, JMcC, CW CS and JG; Supervision, JMcC and CW.

Competing interests – The authors declare that they have no competing interests

Figure Legends

Figure 1 - CCh evoked Ca^{2+} signals in the endothelium of intact arteries. (A) Ai Representative image frame showing ~200 endothelial cells from an imaging field. (Aii) An image of cells with automatically identified regions of interest (ROI) superimposed onto the imaging field of view. (Aiii) Ca^{2+} images illustrating the endothelial response during treatment with CCh (100nM) overlaid on a basal Ca^{2+} image. (B) Expanded view of the endothelium from the area highlighted in the red box in (A). (C) Baseline-corrected Ca^{2+} signals (F/F_0) obtained from the fluorescence within the ROI shown in (B). The color for each trace matches that presented in the ROI in B. The fluorescence amplitudes are scaled in the same way for each cell. (D) Overlaid Ca^{2+} signals from all individual cells identified in Aii. The black line shows the mean response (E) An example single endothelial cell Ca^{2+} signal and the corresponding images shown in F with time-points indicated by the roman numerals (E,F). Scale bars = 50μm

Figure 2 Concentration-dependence of CCh-evoked endothelial Ca^{2+} signaling. (A) Representative composite images of endothelial Ca^{2+} activity in response to increasing concentrations of CCh. The three images show illustrative data from a single artery in which the endothelium was stimulated with consecutively increasing concentrations of CCh. The full series applied in each experiment was 10 increments from 1 nM to 30 μM. Scale bars = 50μm. (B) Average Ca^{2+} (F/F_0) responses from all cells for each concentration of the full series. The individual traces are color-coded based on the concentration of CCh applied. (C) Ca^{2+} traces from a single cell. The color code is the same as shown in B. (D) Percentage of cells activated by increasing concentrations of CCh. The x-axis is $\log_{10}$ of the CCh concentration. (E) Ca^{2+} traces from all 129 individual cells from the datasets shown in A. The black line is the mean response. The other colors assigned to each trace is based on the amplitude of the initial response to CCh in each cell at the highest CCh concentration (right-most dataset), i.e. if a cell's trace is colored blue in one set of traces, the same trace in the other two data sets is also colored blue. The color of each specific cell's trace is maintained throughout subsequent additions of agonist allowing for a direct comparison of the same cells between responses

Figure 3 CCh activates M3 receptors in the endothelium (A) Representative experiment (average of all cells) showing the effect of the selective M3 antagonist 4-DAMP (100 nM). The endothelium was activated by CCh at a concentration (100 μM) evoking a maximum response. Two control responses show approximately reproducible responses. CCh application is indicated by the line above the traces. 4-DAMP inhibits the response. After block of M3 receptors, the cells remain viable and respond to ATP (100 μM; right-hand trace). (B) Composite Ca^{2+} images showing the cells that respond to CCh (100 μM; green) and an absence of response after the block of M3 receptors by 4-DAMP (100 nM). The subsequent application of ATP (100 μM) evoked a response (red). All images are from the same field of endothelium. (C) Ca^{2+} signals from all activated cells in B, 30s baseline and 60s activation. Responses are overlaid and the black line is the average. (D) Paired peak Ca^{2+} (F/F_0) responses from each individual cells (circles) matched for each treatment (grey line) from a single experiment. Average response indicated by white circle and matched across each treatment by bold line. The Plotting Density (right axis) indicates the distribution of Peak F/F_0 values (red high, blue low occurrence of the same value). (E) Paired summary data illustrating changes in Peak F/F_0 response values averaged across all cells (n=5). All Scale bars = 50μm. $p < 0.05$

Figure 4 Concentration-dependence of ATP-evoked endothelial Ca^{2+} signaling. (A) Representative composite images of Ca^{2+} activity in carotid artery endothelium in response to stimulation with increasing concentrations of ATP. The three images show illustrative data from a single experiment in which the endothelium was stimulated with consecutively increasing concentration of ATP (from 100 nM to 10 mM). Scale bars = 50μm. (B) Average Ca^{2+} (F/F_0) responses from all cells in (A). The data shows responses to each concentration of the full series shown in A. The individual traces are color-coded based on the concentration of ATP applied (inset). (C) Ca^{2+} traces from a single cell. Color code is the same as shown in B. (D) Percentage of cells activated by increasing concentrations of ATP. The x-axis is $\log_{10}$ of the CCh concentration. (E) Ca^{2+} traces corresponding to the datasets shown in A. Ca^{2+} signals from all 153 individual cells are shown. The color assigned to each trace is based on the amplitude of the initial response to ATP in each cell at the highest ATP concentration (right-most dataset), i.e. if a cell's trace is colored blue in one set of traces, the same trace in the other data sets is also colored blue.

Figure 5 The initial response to ATP persists in a Ca^{2+} free bath solution (A) Composite Ca^{2+} images showing the cells that respond to ATP (EC_{25}; red) were reproducible and the response persisted when extracellular Ca^{2+} was removed. Two control responses (A, left panels; control and repeat 1) were followed by activation by ATP (EC25) after a 7 minute period in a Ca^{2+} free bath solution. In the Ca^{2+} free bath, the response to ATP was largely unaltered. In the final part of the experiment (repeat 2) Ca^{2+} was restored to the bathing solution and once again a similar response occurred. All images are from the same field of endothelium. (B) Ca^{2+} signals from the activated cells in A, 30s baseline and 60s ATP activation. All traces from individual cells are overlaid and the black line is the average. Time of activation is shown above the trace. (C) Peak Ca^{2+} (F/F_0) response from each individual cells (circle) matched for each treatment (grey line) from a single experiment. Average response indicated by white circle and matched across each treatment by bold line. The Plotting Density (right axis) indicates the distribution of Peak F/F_0 values. (D) Late (steady-state) (F/F_0) response measured at 45 s in controls, after removal of external Ca^{2+} and after the return of extracellular Ca^{2+}. (E) Average peak and steady state responses to ATP (EC_{25}) in control (red) and after removal of external Ca^{2+} (blue); (n=5, $p>0.05$). (F) Composite Ca^{2+} images showing the cells that respond ATP (EC_{75}; red) concentration which also was reproducible and the initial response persisted when extracellular Ca^{2+} was removed. Two control responses (A, left panels; control and repeat 1) were followed by activation by ATP (EC75) after a 7 minute period in a Ca^{2+} free bath solution. In the Ca^{2+} free bath, the response to ATP was largely unaltered. In the final part of the experiment Ca^{2+} was restored to the bathing solution and once again a similar response occurred. All images are from the same field of endothelium. (G) Ca^{2+} signals from the activated cells in F, 30s baseline and 60s ATP activation. All traces from individual cells are overlaid and the black line is the average. Time of activation is shown above the trace. (H) Peak Ca^{2+} (F/F_0) response from each individual cells (circle) matched for each treatment (grey line) from a single experiment. Average response indicated by white circle and matched across each treatment by bold line. The Plotting Density (right axis) indicates the distribution of Peak F/F_0 values. (I) Late (steady-state) (F/F_0) response measured at 45 s in controls, after removal of external Ca^{2+} and after the return of extracellular Ca^{2+}. (J) Average peak and steady state responses to ATP (EC_{25}) in control (red) and after removal of external Ca^{2+} (blue); (n=5, $p>0.05$ for the peak response; $p<0.05$ for the late response). All scale bars = 50 μm.

Figure 6 ATP activates P2Y2 receptors in the endothelium (A) Representative experiment showing the effect of the P2Y1 antagonist MRS2179 (10 μM) and P2Y2 antagonist ARC118925 (1 μM) on the maximal response to ATP (100 μM). The traces show the average responses from all cells in the field. The P2Y1 antagonists (MRS2179, 10 μM) had only a small effect on the response. The responses are almost fully blocked by the P2Y2 receptor blocker (ARC118925; 1 μM). The small residual response is inhibited by the P2Y1 antagonist. At the end of the experiment CCh (100 μM) was applied to confirm cell viability. (B) Composite Ca^{2+} images showing the cells that respond to ATP (100 μM) in presence of MRS2179 or ARC118925 (red) or both. The right panel shows the cells that response to CCh (100 μM; green) at the end of the experiment. All images are from the same field of endothelium. (C) Ca^{2+} signals from the activated cells in B, 30s baseline and 60s activation are shown. (D) Peak Ca^{2+} (F/F_0) response from each individual cell (circle) matched for each treatment (grey line) from a single experiment. Average response indicated by white circle and matched across each treatment by bold line. The Plotting Density (right-hand axis) indicates the distribution of Peak F/F_0 values (red high, blue low occurrence of the same values). (E) Paired summary data illustrating changes in Peak F/F_0 response values averaged across all cells. Each color represents a different animal and is maintained across the different treatments (n=5). All Scale bars = 50μm. $p < 0.05$

Figure 7 Agonists activate spatially-distinct clusters of cells. (A) Representative composite images of Ca^{2+} activity in the endothelium in response to the EC_{25} and EC_{75} concentrations of CCh and ATP in a single artery. The first responding (initial 4s; Ai) and total number of cells (Aii) activated by the EC_{25} and EC_{75} of CCh and ATP are shown. Images are scaled to show all activated cells. (B) The number of activated cells and their spatial relationships were calculated from Voronoi neighor analysis and presented as 'Star maps'. The plot shows the cells in the first 4s of activation (dots and lines) by CCh and ATP from the total population of cells (grey crosses and cell outlines). The star map shows the same data presented in A (first responding). (C,D) plots the number of neighboring cells activated by the EC_{25} and EC_{75} of ATP and CCh in the first 4 s (C) and total cells activated over the entire data set (D). The total number of neighbors was determined for each cell from the Voronoi neighbor analysis (6; black circles) and number of these activated for each of the conditions (red circles) is significantly greater ($p<0.05$) from that predicted from a random model of activated cells (blue circles). The expectation of the number of neighbors activated randomly was determined as the (mean number of neighbours) * (activating fraction) for each agonist. (E) Number of cells activated at the concentration shown on the x-axis as a percentage of the total population of cells in the field (red and left). "First responding cells" are the cells activated within the first 4s. The right side of each plot (E; blue) shows the percentage of precisely the same cells that are activated by each of the conditions shown. The plot shows that those cells that are most sensitive to one agonist are much less sensitive to the other. (F) The number of clusters and number of cells in a cluster increase at the EC_{75} when compared to the EC_{25} of CCh and ATP. All Scale bars = 50μm.

Figure 8 Heterogenous distribution of muscarinic and purinergic receptors. (A) Fluorescence localization of purinergic P2Y2 receptors and muscarinic M3 receptors in the endothelium. Representative images (from left) show the endothelial cell boundaries as revealed by PECAM-1 labelling (green; anti- CD31/PECAM-1), P2Y2 receptor (red; anti-P2Y2) distribution, M3 receptor distribution (green; fluorescent M3 receptor antagonist, 100 nM) and overlay of all three. The receptors distribution was not uniform across the endothelium and there was relatively little overlap of purinergic and muscarinic receptor staining. (B) Expanded view of the endothelial images shown in A. The expanded region is shown by the red box in A left-

panel. (C) Negative control. The left panel is again PECAM-1 labeled to show cell boundary positions. The negative control for P2Y2 staining was obtained by omitting the primary antibody against P2Y2. The control for M3 staining was obtained by labelling with the fluorescent M3 receptor ligand in the presence of the M3 receptor antagonist 4-DAMP (10 μM). The right panel shows an overlay of all three. (D) Summary data showing the levels of M3 staining in the presence and absence of the antagonist 4-DAMP (green), the extent of labelling in the presence and absence of the P2Y2 primary antibody (red); and the extent of overlap of specific M3 and P2Y2 staining (grey). (E) Summary data showing the percentage of cells with M3 staining (green), P2Y2 receptor staining (red) and the percentage of cells expressing both M3 and P2Y2 receptor staining (grey) (n = 3, *p < 0.05, unpaired t-test). All scale bars = 50 μm.

Figure 9 Signal integration and parallel processing. (A) Composite Ca^{2+} images showing cells that respond in the first 4 seconds of activation by the EC_{25} concentrations of CCh (left, green) and ATP (middle, red). Images are of the same field of endothelium. The right-panel shows cells activated (cyan) in the same field of endothelium when both drugs were applied together. (B) Ca^{2+} responses from all activate cells in the field of endothelium shown in A. The Ca^{2+} increase evoked by CCh was on average a slow increase that remained elevated with oscillations (left green). The response to ATP on average was a sharp transient increase that declined towards resting values (red middle). When both agonist were applied (combined; blue right) the Ca^{2+} increase appeared to have features of each agonist i.e. a slow but larger initial increase than with CCh, which remained more elevated than ATP and slowly declined. Agonists were present for the duration indicated by the line above each trace. (C) Examples of responses from 3 separate cells to CCh, ATP and to the two agonists when applied together. In each panel in C, traces are from the cells indicated by the white dots in the panels in A. It is the same 3 cells in each case. Cell 1 is shown in the left panel in C, cell 2 in the middle panel and cell 3 in the right panel. Cell 1 (left panel) responds to CCh but not to ATP. The characteristics of the response in Cell 1 is altered when both ATP and CCh are present (combined) with a faster and larger upstroke. Cell 2 responds to ATP but not CCh. Once again the characteristics of the response in Cell 2 is altered when both ATP and CCh are present (combined) with a more sustained later Ca^{2+} change. Cell 3 responds to each agonist (CCh and to ATP). Once again the characteristics of the response in Cell 3 is altered when both ATP and CCh are present (combined). (D) Mean peak responses (black circles) to the EC_{25} of CCh and ATP separately and when both were present together (combined). The red line shows the calculated mean of peak response when both agonists were added separately. The red shaded region shows the standard error of the mean. The blue line shows the sum of the peak responses when both agonists were added separately. The blue shaded region shows the standard error of the mean. The combined peak response exceeded the mean and was less than the summed response. (D) Mean steady-state responses (black circles) to the EC_{25} of CCh and ATP separately and when both were present together (combined). The red line shows the calculated mean of the steady-state response when both agonists were added separately. The red shaded region shows the standard error of the mean. The blue line shows the sum of the steady-state responses when both agonists were added separately. The blue shaded region shows the standard error of the mean. The combined steady-state response exceeded both the mean and the summed response. All Scale bars = 50μm.

Figure 10 Signals integration and communication across cells (A) Composite Ca^{2+} images showing cells that respond in the first 4 seconds of activation to the EC_{25} and EC_{75} concentrations of CCh (green) and ATP (red) and the response to the EC_{25} concentrations of CCh and ATP

when added together (combined; cyan). All images are from the same field of endothelium. (B) Ca^{2+} responses from the activated cells in A show 30s of baseline and 60s of activation. (C,D) A zoomed region (red box in A) of an example cell (yellow line) that is largely unresponsive to a low (EC_{25}; D light green) or a high concentration of CCh (EC_{75}; D, dark green). The same cell responded to ATP EC_{25} (D, light red) and ATP EC_{75} (D, dark red). The cell's response to ATP EC_{25} was substantially increased when the EC_{25} of CCh was also present (right panel, cyan) and remained elevated when compared to ATP (EC_{25}) in the absence of CCh. All Scale bars = 50μm.

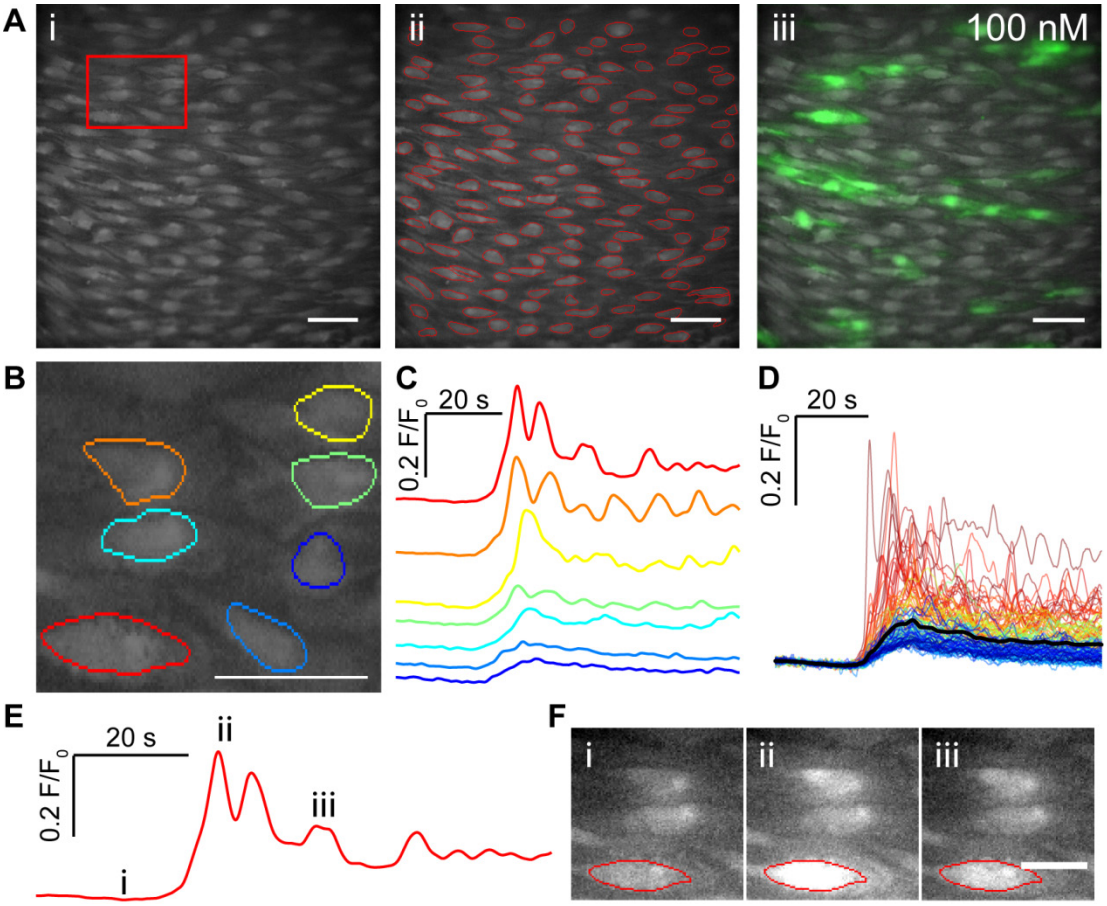

Figure 1 - CCh evoked Ca^{2+} signals in the endothelium of intact arteries. (A) Ai Representative image frame showing ~200 endothelial cells from an imaging field. (Aii) An image of cells with automatically identified regions of interest (ROI) superimposed onto the imaging field of view. (Aiii) Ca^{2+} images illustrating the endothelial response during treatment with CCh (100nM) overlaid on a basal Ca^{2+} image. (B) Expanded view of the endothelium from the area highlighted in the red box in (A). (C) Baseline-corrected Ca^{2+} signals (F/F_0) obtained from the fluorescence within the ROI shown in (B). The color for each trace matches that presented in the ROI in B. The fluorescence amplitudes are scaled in the same way for each cell. (D) Overlaid Ca^{2+} signals from all individual cells identified in Aii. The black line shows the mean response (E) An example single endothelial cell Ca^{2+} signal and the corresponding images shown in F with time-points indicated by the roman numerals (E,F). Scale bars = 50µm.

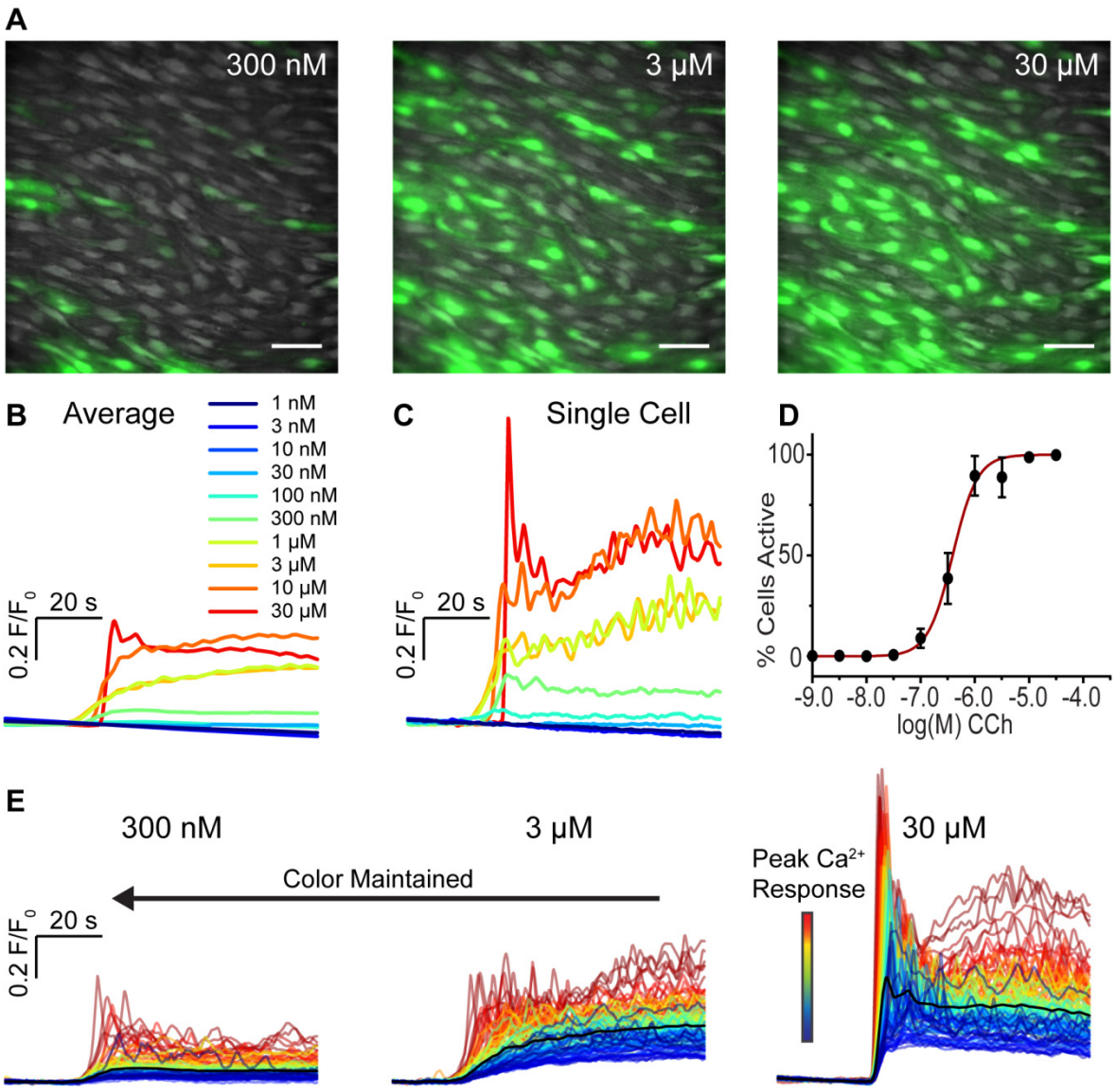

Figure 2 Concentration-dependence of CCh-evoked endothelial Ca^{2+} signaling. (A) Representative composite images of endothelial Ca^{2+} activity in response to increasing concentrations of CCh. The three images show illustrative data from a single artery in which the endothelium was stimulated with consecutively increasing concentrations of CCh. The full series applied in each experiment was 10 increments from 1 nM to 30 µM. Scale bars = 50µm. (B) Average Ca^{2+} (F/F_0) responses from all cells for each concentration of the full series. The individual traces are color-coded based on the concentration of CCh applied. (C) Ca^{2+} traces from a single cell. The color code is the same as shown in B. (D) Percentage of cells activated by increasing concentrations of CCh. The x-axis is $\log_{10}$ of the CCh concentration. (E) Ca^{2+} traces from all 129 individual cells from the datasets shown in A. The black line is the mean response. The other colors assigned to each trace is based on the amplitude of the initial response to CCh in each cell at the highest CCh concentration (right-most dataset), i.e. if a cell's trace is colored blue in one set of traces, the same trace in the other two data sets is also colored blue. The color of each specific cell's trace is maintained throughout subsequent additions of agonist allowing for a direct comparison of the same cells between responses.

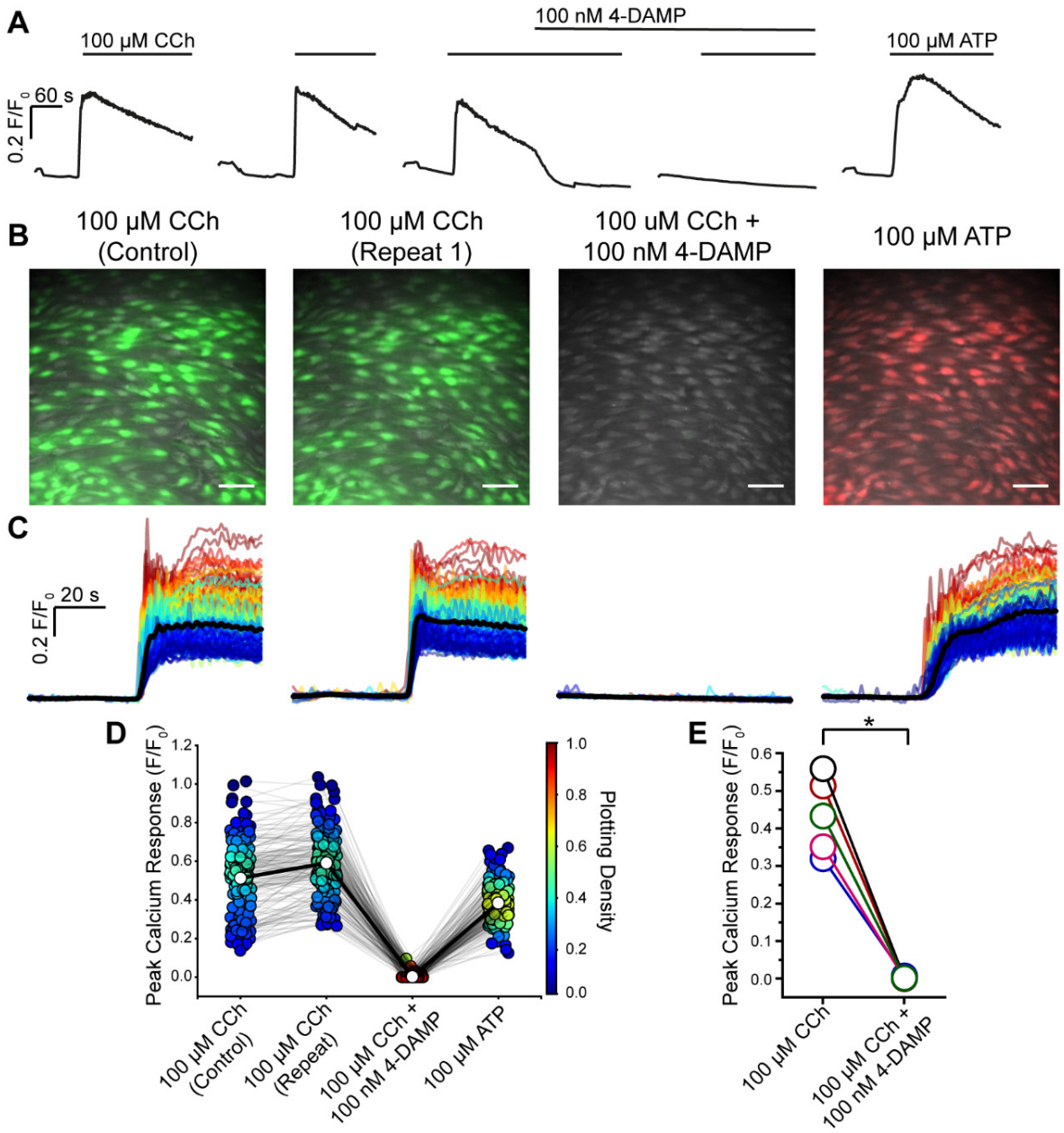

Figure 3 CCh activates M3 receptors in the endothelium (A) Representative experiment (average of all cells) showing the effect of the selective M3 antagonist 4-DAMP (100 nM). The endothelium was activated by CCh at a concentration (100 µM) evoking a maximum response. Two control responses show approximately reproducible responses. CCh application is indicated by the line above the traces. 4-DAMP inhibits the response. After block of M3 receptors, the cells remain viable and respond to ATP (100 µM; right-hand trace). (B) Composite Ca^{2+} images showing the cells that respond to CCh (100 µM; green) and an absence of response after the block of M3 receptors by 4-DAMP (100 nM). The subsequent application of ATP (100 µM) evoked a response (red). All images are from the same field of endothelium. (C) Ca^{2+} signals from all activated cells in B, 30s baseline and 60s activation. Responses are overlaid and the black line is the average. (D) Paired peak Ca^{2+} (F/F_0) responses from each individual cells (circles) matched for each treatment (grey line) from a single experiment. Average response indicated by white circle and matched across each treatment by bold line. The Plotting Density (right axis) indicates the distribution of Peak F/F_0 values (red high, blue low occurrence of the same value). (E) Paired summary data illustrating changes in Peak F/F_0 response values averaged across all cells (n=5). All Scale bars = 50µm. $p < 0.05$.

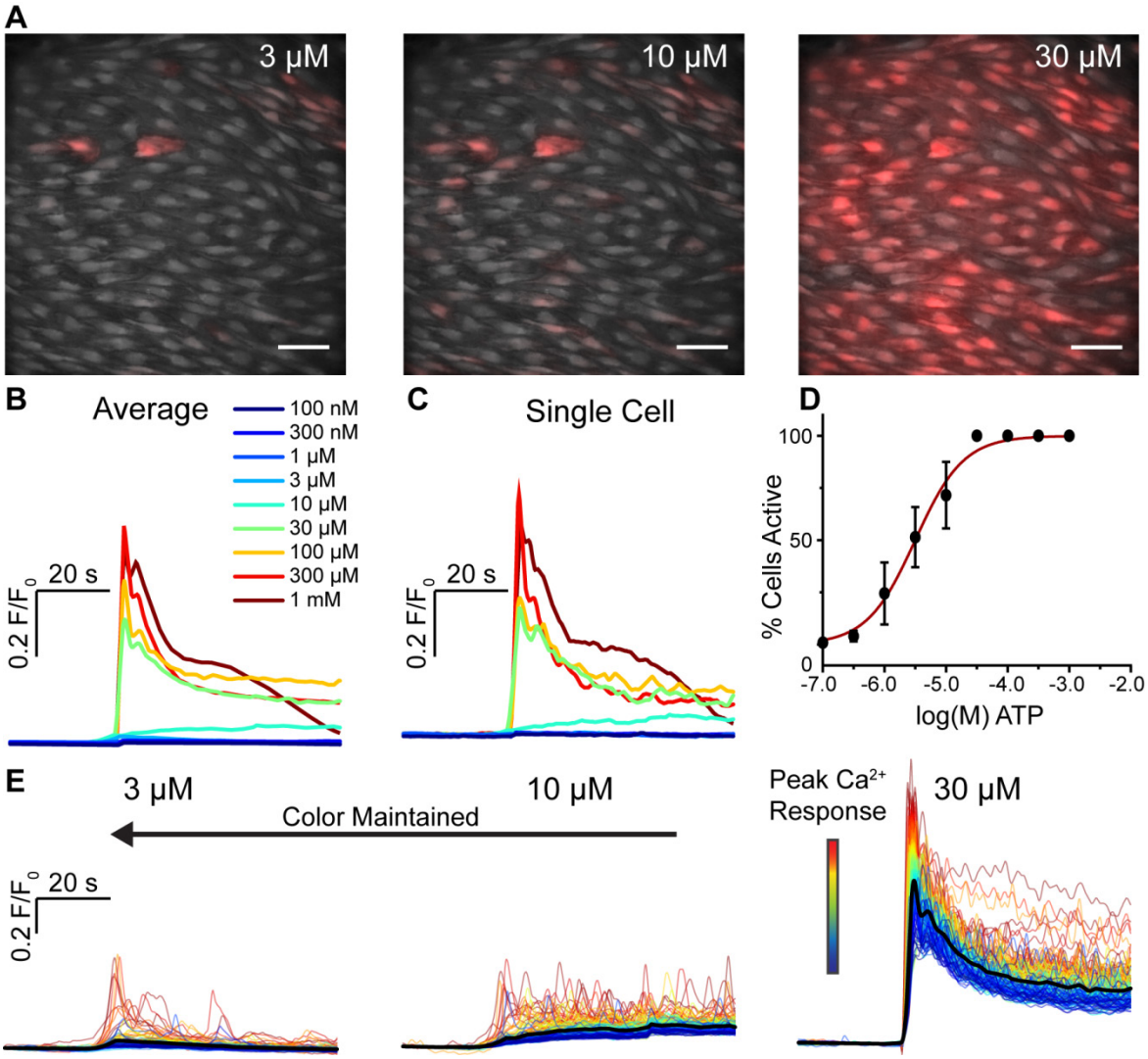

Figure 4 Concentration-dependence of ATP-evoked endothelial Ca^{2+} signaling. (A) Representative composite images of Ca^{2+} activity in carotid artery endothelium in response to stimulation with increasing concentrations of ATP. The three images show illustrative data from a single experiment in which the endothelium was stimulated with consecutively increasing concentration of ATP (from 100 nM to 10 mM). Scale bars = 50µm. (B) Average Ca^{2+} (F/F_0) responses from all cells in (A). The data shows responses to each concentration of the full series shown in A. The individual traces are color-coded based on the concentration of ATP applied (inset). (C) Ca^{2+} traces from a single cell. Color code is the same as shown in B. (D) Percentage of cells activated by increasing concentrations of ATP. The x-axis is $\log_{10}$ of the CCh concentration. (E) Ca^{2+} traces corresponding to the datasets shown in A. Ca^{2+} signals from all 153 individual cells are shown. The color assigned to each trace is based on the amplitude of the initial response to ATP in each cell at the highest ATP concentration (right-most dataset), i.e. if a cell's trace is colored blue in one set of traces, the same trace in the other data sets is also colored blue.

.

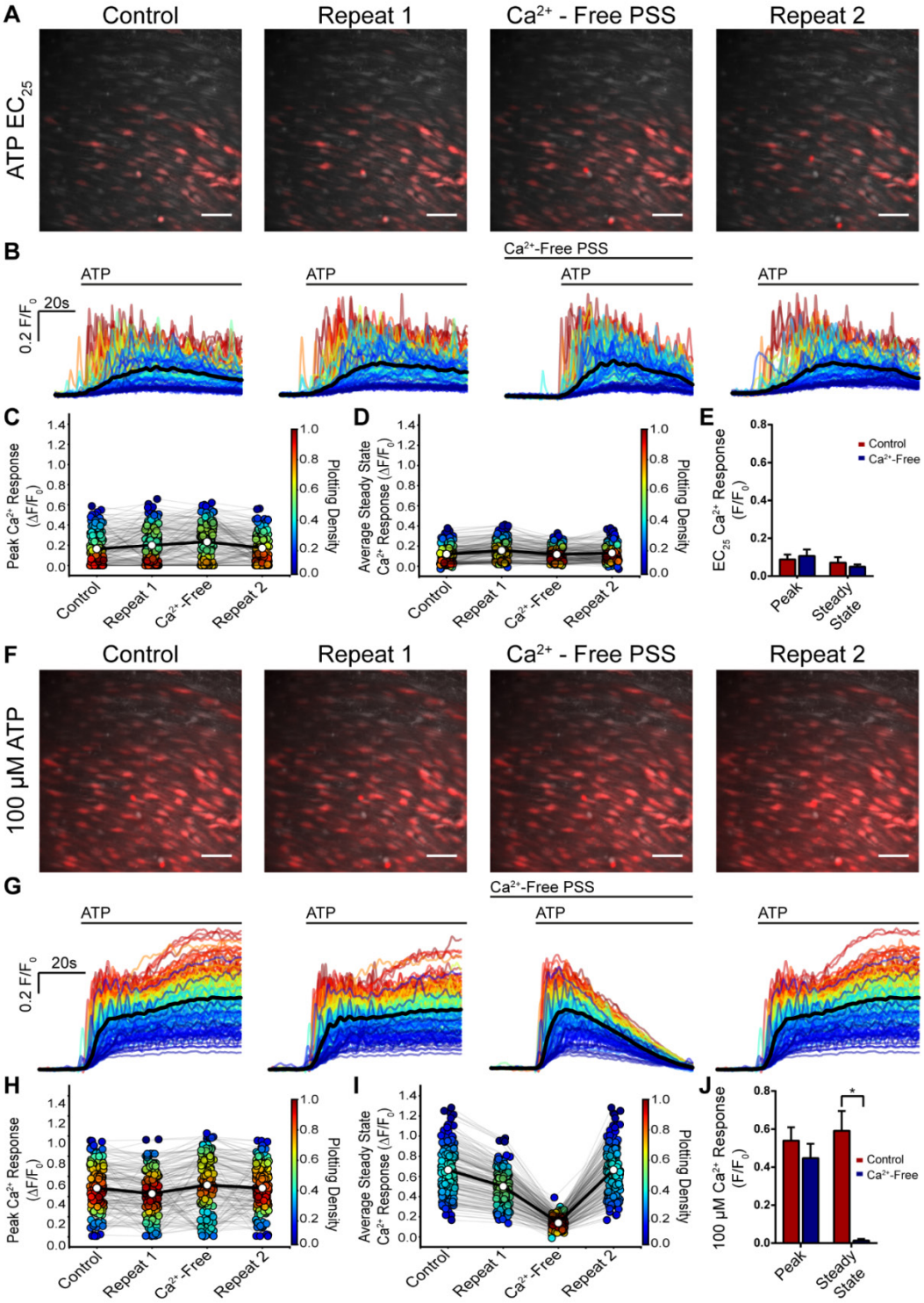

Figure 5 The initial response to ATP persists in a Ca^{2+} free bath solution (A) Composite Ca^{2+} images showing the cells that respond to ATP (EC_{25}; red) were reproducible and the response persisted when extracellular Ca^{2+} was removed. Two control responses (A, left panels; control and repeat 1) were followed by activation by ATP (EC25) after a 7 minute period in a Ca^{2+} free bath solution. In the Ca^{2+} free bath, the response to ATP was largely unaltered. In the final part of the experiment (repeat 2) Ca^{2+} was restored to the bathing solution and once again a similar response occurred. All images are from the same field of endothelium. (B) Ca^{2+} signals from the activated cells in A, 30s baseline and 60s ATP

activation. All traces from individual cells are overlaid and the black line is the average. Time of activation is shown above the trace. (C) Peak Ca^{2+} (F/F_0) response from each individual cells (circle) matched for each treatment (grey line) from a single experiment. Average response indicated by white circle and matched across each treatment by bold line. The Plotting Density (right axis) indicates the distribution of Peak F/F_0 values. (D) Late (steady-state) (F/F_0) response measured at 45 s in controls, after removal of external Ca^{2+} and after the return of extracellular Ca^{2+}. (E) Average peak and steady state responses to ATP (EC_{25}) in control (red) and after removal of external Ca^{2+} (blue); (n=5, $p>0.05$). (F) Composite Ca^{2+} images showing the cells that respond ATP (EC_{75}; red) concentration which also was reproducible and the initial response persisted when extracellular Ca^{2+} was removed. Two control responses (A, left panels; control and repeat 1) were followed by activation by ATP (EC75) after a 7 minute period in a Ca^{2+} free bath solution. In the Ca^{2+} free bath, the response to ATP was largely unaltered. In the final part of the experiment Ca^{2+} was restored to the bathing solution and once again a similar response occurred. All images are from the same field of endothelium. (G) Ca^{2+} signals from the activated cells in F, 30s baseline and 60s ATP activation. All traces from individual cells are overlaid and the black line is the average. Time of activation is shown above the trace. (H) Peak Ca^{2+} (F/F_0) response from each individual cells (circle) matched for each treatment (grey line) from a single experiment. Average response indicated by white circle and matched across each treatment by bold line. The Plotting Density (right axis) indicates the distribution of Peak F/F_0 values. (I) Late (steady-state) (F/F_0) response measured at 45 s in controls, after removal of external Ca^{2+} and after the return of extracellular Ca^{2+}. (J) Average peak and steady state responses to ATP (EC_{25}) in control (red) and after removal of external Ca^{2+} (blue); (n=5, $p>0.05$ for the peak response; $p<0.05$ for the late response). All scale bars = 50 μm

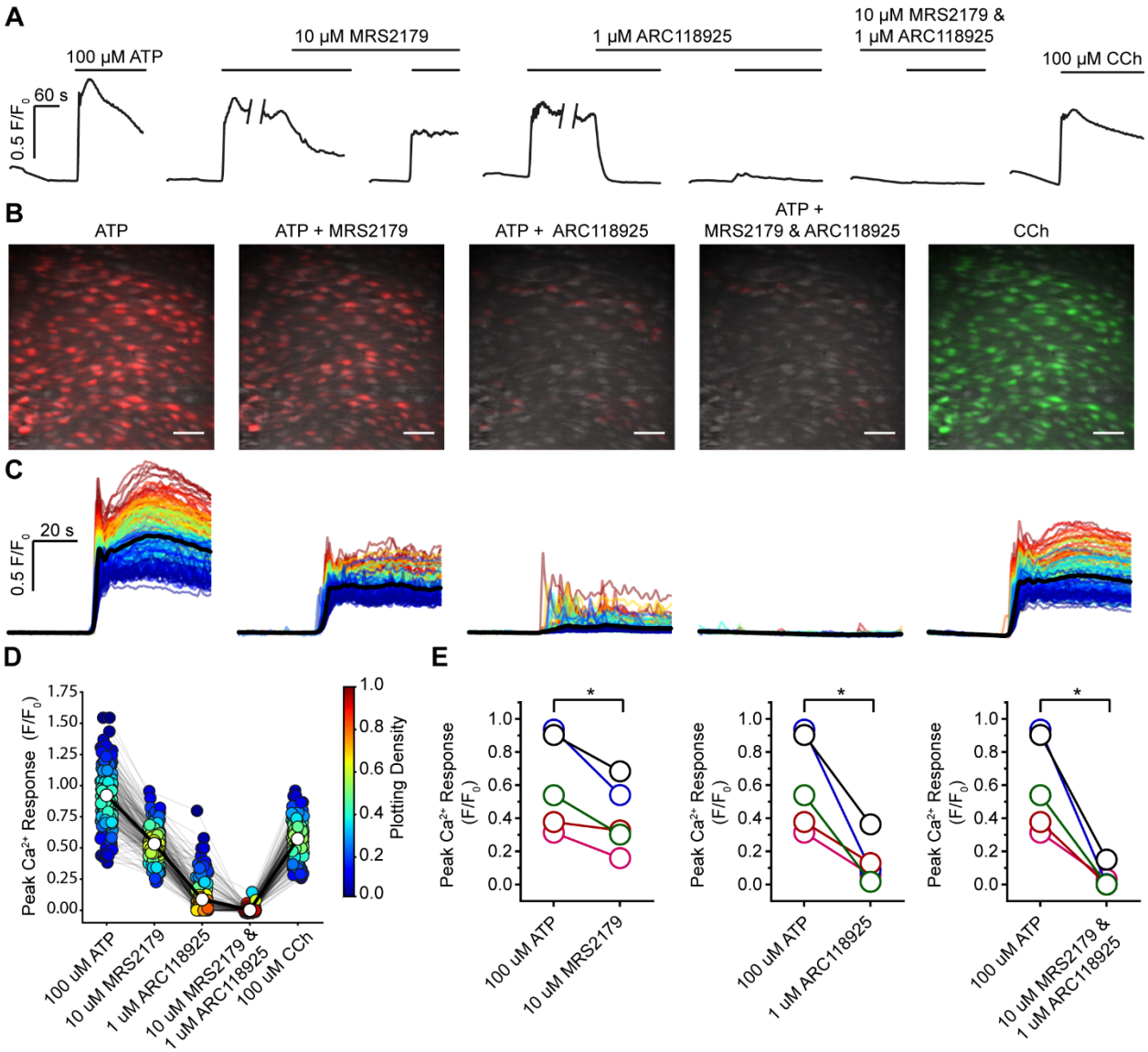

Figure 6 ATP activates P2Y2 receptors in the endothelium (A) Representative experiment showing the effect of the P2Y1 antagonist MRS2179 (10 µM) and P2Y2 antagonist ARC118925 (1 µM) on the maximal response to ATP (100 µM). The traces show the average responses from all cells in the field. The P2Y1 antagonists (MRS2179, 10 µM) had only a small effect on the response. The responses are almost fully blocked by the P2Y2 receptor blocker (ARC118925; 1 µM). The small residual response is inhibited by the P2Y1 antagonist. At the end of the experiment CCh (100 µM) was applied to confirm cell viability. (B) Composite Ca^{2+} images showing the cells that respond to ATP (100 µM) in presence of MRS2179 or ARC118925 (red) or both. The right panel shows the cells that response to CCh (100 µM; green) at the end of the experiment. All images are from the same field of endothelium. (C) Ca^{2+} signals from the activated cells in B, 30s baseline and 60s activation are shown. (D) Peak Ca^{2+} (F/F_0) response from each individual cell (circle) matched for each treatment (grey line) from a single experiment. Average response indicated by white circle and matched across each treatment by bold line. The Plotting Density (right-hand axis) indicates the distribution of Peak F/F_0 values (red high, blue low occurrence of the same values). (E) Paired summary data illustrating changes in Peak F/F_0 response values averaged across all cells. Each color represents a different animal and is maintained across the different treatments (n=5). All Scale bars = 50µm. $p < 0.05$.

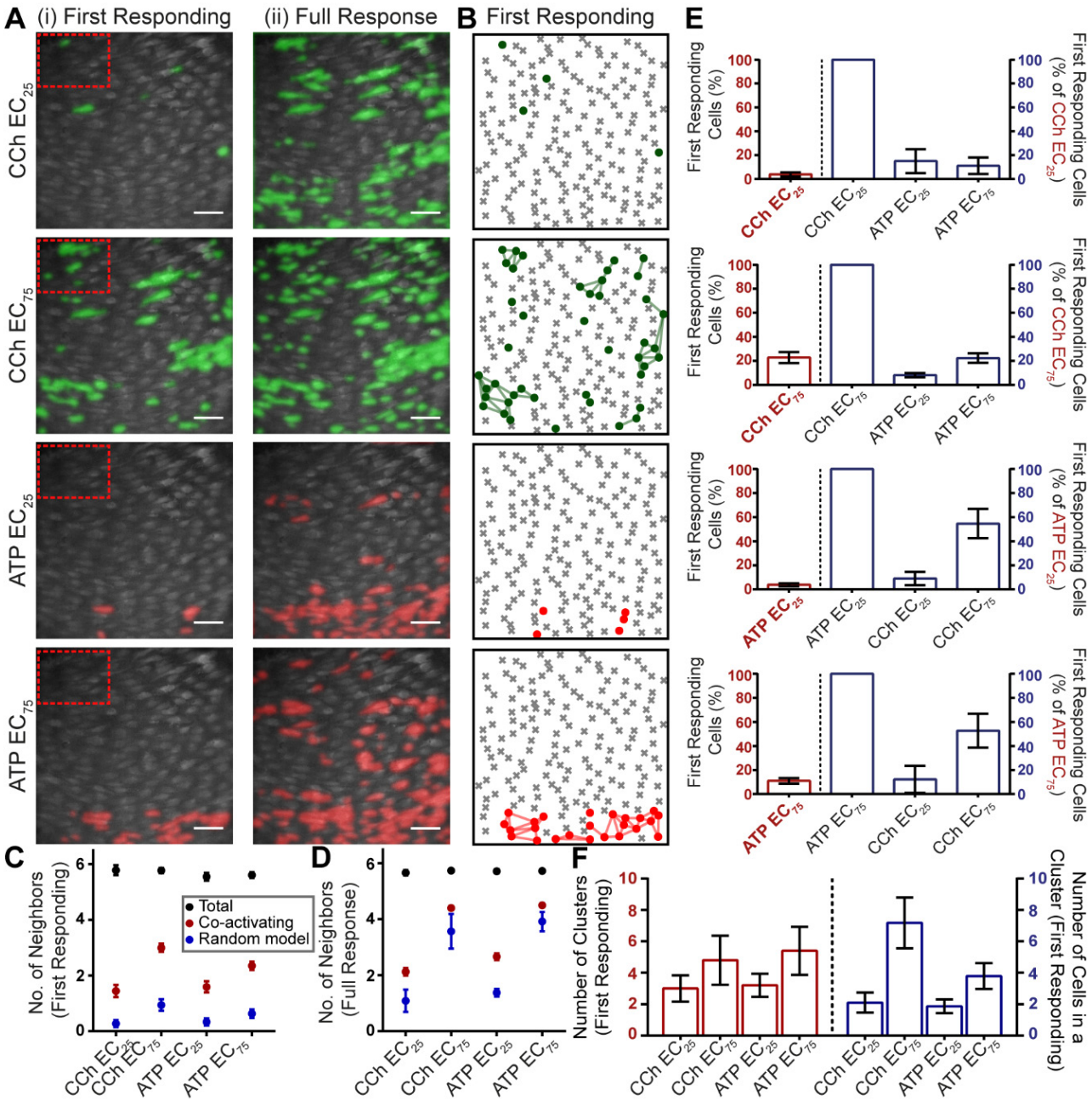

Figure 7 Agonists activate spatially-distinct clusters of cells. (A) Representative composite images of Ca^{2+} activity in the endothelium in response to the EC_{25} and EC_{75} concentrations of CCh and ATP in a single artery. The first responding (initial 4s; Ai) and total number of cells (Aii) activated by the EC_{25} and EC_{75} of CCh and ATP are shown. Images are scaled to show all activated cells. (B) The number of activated cells and their spatial relationships were calculated from Voronoi neighbor analysis and presented as 'Star maps'. The plot shows the cells in the first 4s of activation (dots and lines) by CCh and ATP from the total population of cells (grey crosses and cell outlines). The star map shows the same data presented in A (first responding). (C,D) plots the number of neighboring cells activated by the EC_{25} and EC_{75} of ATP and CCh in the first 4 s (C) and total cells activated over the entire data set (D). The total number of neighbors was determined for each cell from the Voronoi neighbor analysis (6; black circles) and number of these activated for each of the conditions (red circles) is significantly greater ($p<0.05$) from that predicted from a random model of activated cells (blue circles). The expectation of the number of neighbors activated randomly was determined as the (mean number

of neighbors) * (activating fraction) for each agonist. (E) Number of cells activated at the concentration shown on the x-axis as a percentage of the total population of cells in the field (red and left). “First responding cells” are the cells activated within the first 4s. The right side of each plot (E; blue) shows the percentage of precisely the same cells that are activated by each of the conditions shown. The plot shows that those cells that are most sensitive to one agonist are much less sensitive to the other. (F) The number of clusters and number of cells in a cluster increase at the EC_{75} when compared to the EC_{25} of CCh and ATP. All Scale bars = 50μm.

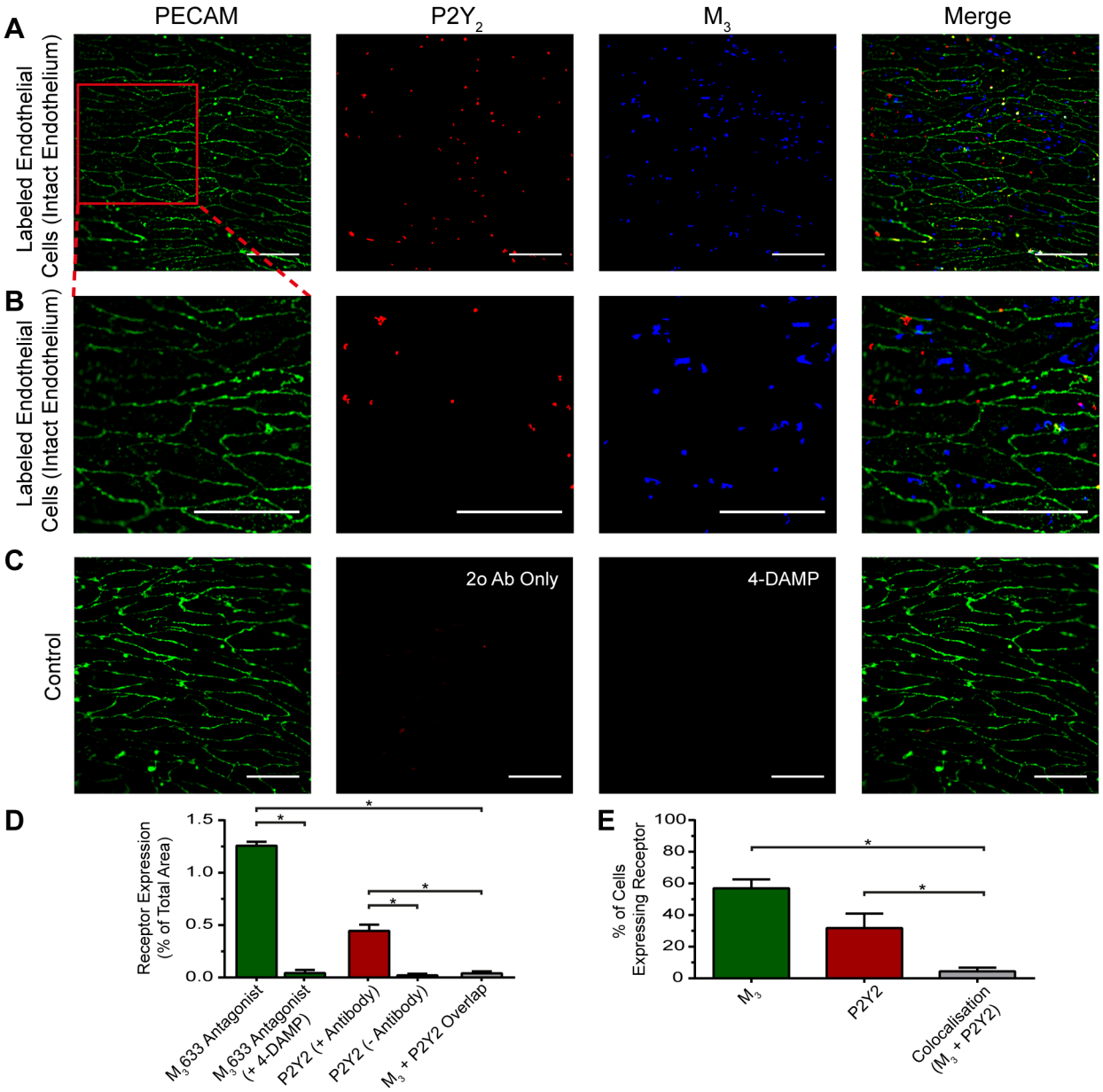

Figure 8 Heterogenous distribution of muscarinic and purinergic receptors. (A) Fluorescence localization of purinergic P2Y2 receptors and muscarinic M3 receptors in the endothelium. Representative images (from left) show the endothelial cell boundaries as revealed by PECAM-1 labelling (green; anti- CD31/PECAM-1), P2Y2 receptor (red; anti-P2Y2) distribution, M3 receptor distribution (green; fluorescent M3 receptor antagonist, 100 nM) and overlay of all three. The receptors distribution was not uniform across the endothelium and there was relatively little overlap of purinergic and muscarinic receptor staining. (B) Expanded view of the endothelial images shown in A. The expanded region is shown by the red box in A left-panel. (C) Negative control. The left panel is again PECAM-1 labeled to show cell boundary positions. The negative control for P2Y2 staining was obtained by omitting the primary antibody against P2Y2. The control for M3 staining was obtained by labelling with the fluorescent M3 receptor ligand in the presence of the M3 receptor antagonist 4-DAMP (10 µM). The right panel shows an overlay of all three. (D) Summary data showing the levels of M3 staining in the presence and absence of the antagonist 4-DAMP (green), the extent of labelling in the presence and

absence of the P2Y2 primary antibody (red); and the extent of overlap of specific M3 and P2Y2 staining (grey). (E) Summary data showing the percentage of cells with M3 staining (green), P2Y2 receptor staining (red) and the percentage of cells expressing both M3 and P2Y2 receptor staining (grey) ($n = 3$, $*p < 0.05$, unpaired t-test). All scale bars = 50 μm.

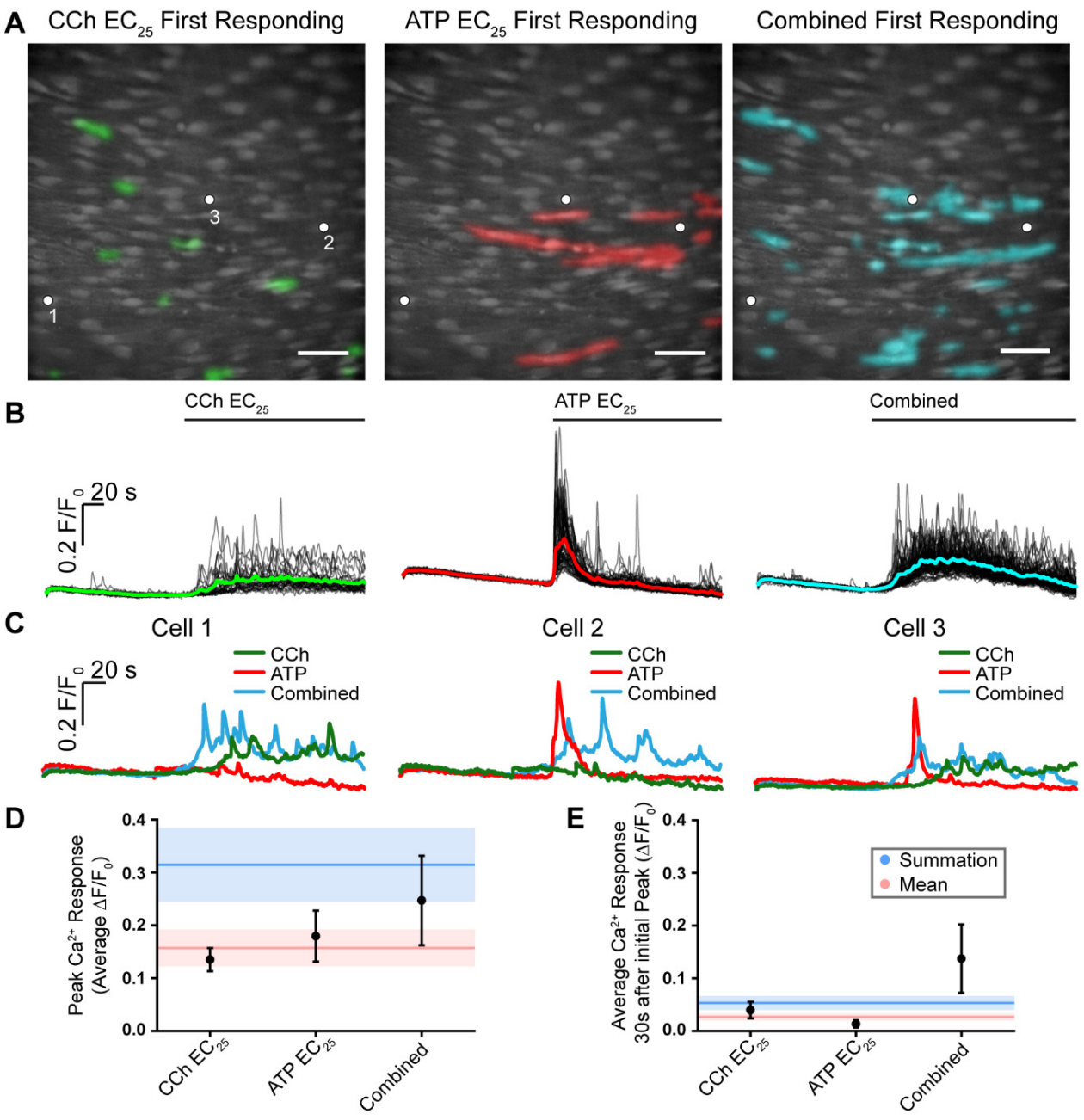

Figure 9 Signal integration and parallel processing. (A) Composite Ca^{2+} images showing cells that respond in the first 4 seconds of activation by the EC_{25} concentrations of CCh (left, green) and ATP (middle, red). Images are of the same field of endothelium. The right-panel shows cells activated (cyan) in the same field of endothelium when both drugs were applied together. (B) Ca^{2+} responses from all activate cells in the field of endothelium shown in A. The Ca^{2+} increase evoked by CCh was on average a slow increase that remained elevated with oscillations (left green). The response to ATP on average was a sharp transient increase that declined towards resting values (red middle). When both agonist were applied (combined; blue right) the Ca^{2+} increase appeared to have features of each agonist i.e. a slow but larger initial increase than with CCh, which remained more elevated than ATP and slowly declined. Agonists were present for the duration indicated by the line above each trace. (C) Examples of responses from 3 separate cells to CCh, ATP and to the two agonists when applied together. In each panel in C, traces are from the cells indicated by the white dots in the panels in A. It is the same 3 cells in each case. Cell 1 is shown in the left panel in C, cell 2 in the middle panel and cell 3

in the right panel. Cell 1 (left panel) responds to CCh but not to ATP. The characteristics of the response in Cell 1 is altered when both ATP and CCh are present (combined) with a faster and larger upstroke. Cell 2 responds to ATP but not CCh. Once again the characteristics of the response in Cell 2 is altered when both ATP and CCh are present (combined) with a more sustained later Ca^{2+} change. Cell 3 responds to each agonist (CCh and to ATP). Once again the characteristics of the response in Cell 3 is altered when both ATP and CCh are present (combined). (D) Mean peak responses (black circles) to the EC_{25} of CCh and ATP separately and when both were present together (combined). The red line shows the calculated mean of peak response when both agonists were added separately. The red shaded region shows the standard error of the mean. The blue line shows the sum of the peak responses when both agonists were added separately. The blue shaded region shows the standard error of the mean. The combined peak response exceeded the mean and was less than the summed response. (D) Mean steady-state responses (black circles) to the EC_{25} of CCh and ATP separately and when both were present together (combined). The red line shows the calculated mean of the steady-state response when both agonists were added separately. The red shaded region shows the standard error of the mean. The blue line shows the sum of the steady-state responses when both agonists were added separately. The blue shaded region shows the standard error of the mean. The combined steady-state response exceeded both the mean and the summed response. All Scale bars = 50μm.

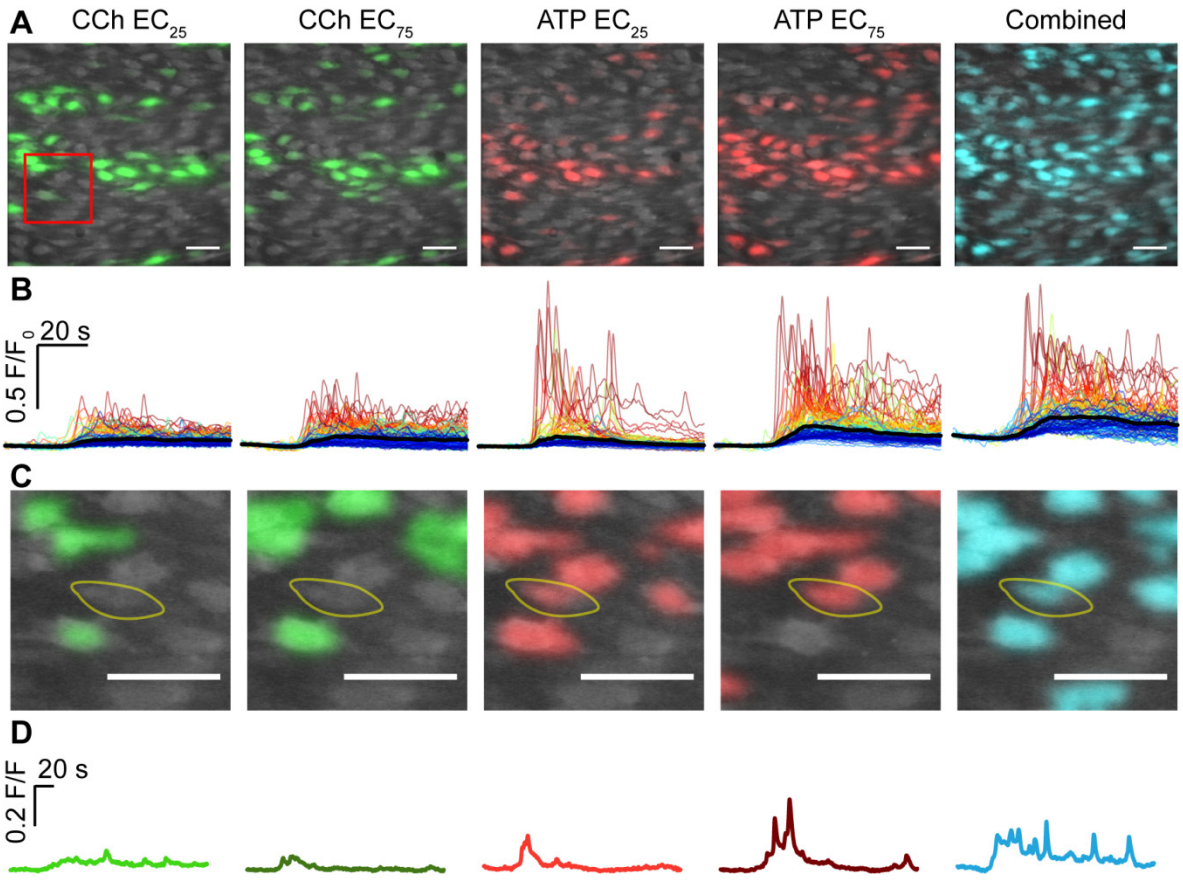

Figure 10 Signals integration and communication across cells (A) Composite Ca^{2+} images showing cells that respond in the first 4 seconds of activation to the EC_{25} and EC_{75} concentrations of CCh (green) and ATP (red) and the response to the EC_{25} concentrations of CCh and ATP when added together (combined; cyan). All images are from the same field of endothelium. (B) Ca^{2+} responses from the activated cells in A show 30s of baseline and 60s of activation. (C,D) A zoomed region (red box in A) of an example cell (yellow line) that is largely unresponsive to a low (EC_{25}; D light green) or a high concentration of CCh (EC_{75}; D, dark green). The same cell responded to ATP EC_{25} (D, light red) and ATP EC_{75} (D, dark red). The cell's response to ATP EC_{25} was substantially increased when the EC_{25} of CCh was also present (right panel, cyan) and remained elevated when compared to ATP (EC_{25}) in the absence of CCh. All Scale bars = 50µm.

SUPPLEMENTARY DATA

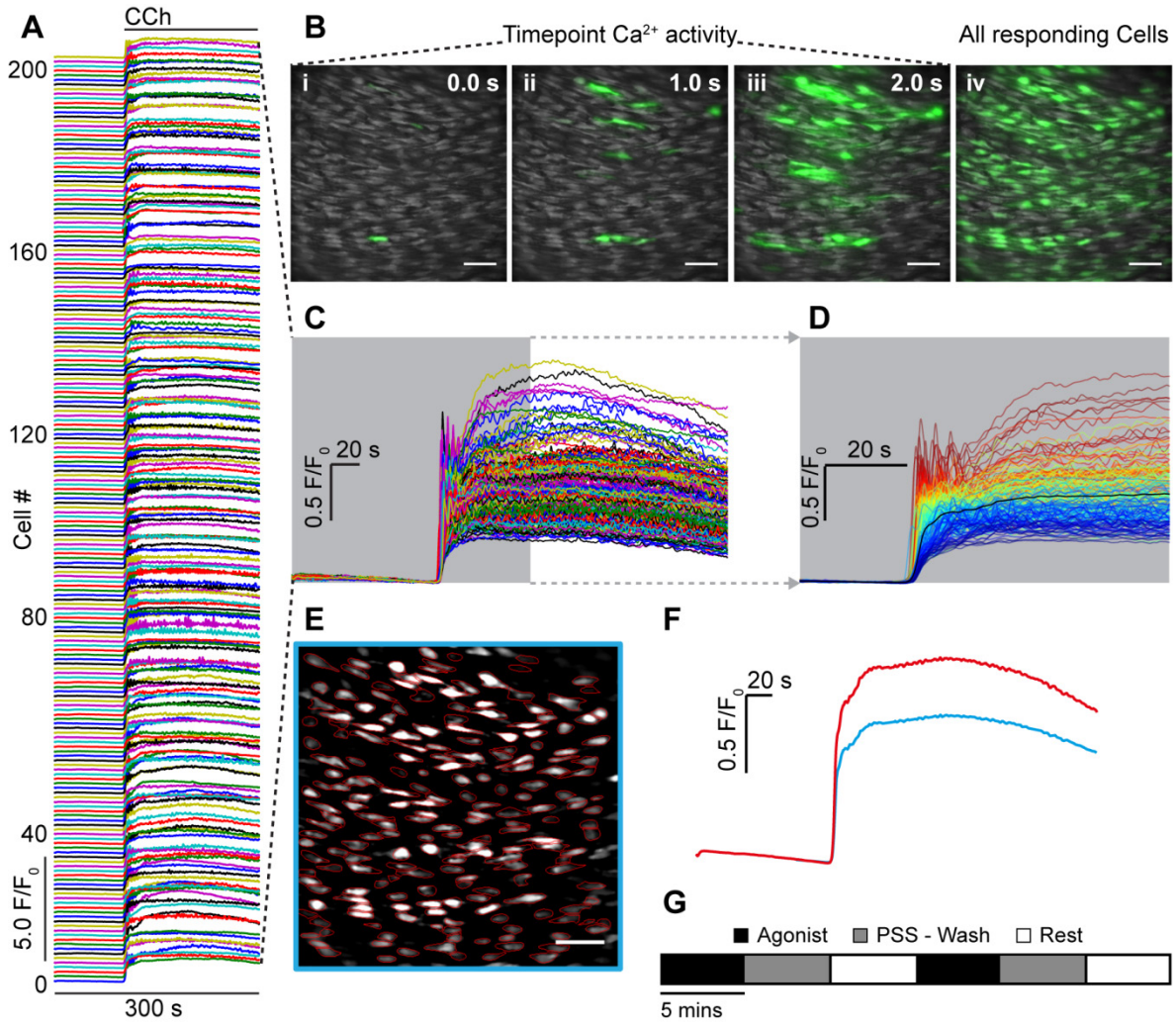

Supplementary Figure S1 CCh evoked Ca^{2+} signals in the endothelium. (A) F/F_0 Ca^{2+} signals for each of the individual cells shown in B, each line is a different cell. (B) Composite Ca^{2+} images illustrating the endothelial response at specific timepoints ($B_{i\text{-}iii}$) during treatment with CCh (10 µM). (B_{iv}) Image showing all responding cells to CCh over the entire recording. (C) F/F_0 Ca^{2+} signals of single cells (from B), overlaid and baseline normalized. (D) Baseline-corrected and time-aligned Ca^{2+} signals (from C), shown over an expanded time-scale (grey region in C). The Ca^{2+} signals have been colored according to the amplitude of the first rise in Ca^{2+}. Red indicates the highest amplitude and blue, the lowest amplitude. (E) Automatically generated regions of interest (ROIs; red) for each cell shown overlaid on a sharpened basal Ca^{2+} image. The blue square surrounding the entire field shows the whole-field ROI used for average analysis shown in F. (F) Baseline-corrected Ca^{2+} signals (F/F0) obtained by averaging fluorescence within the whole field ROI (blue) and by average each cellular Ca^{2+} signal (red). (G) Schematic indicating the timing of agonist addition, wash and recovery used in the experiments. During each agonist addition there was a 2 min recording of baseline followed by 3 min of activation. Scale bars = 50µm

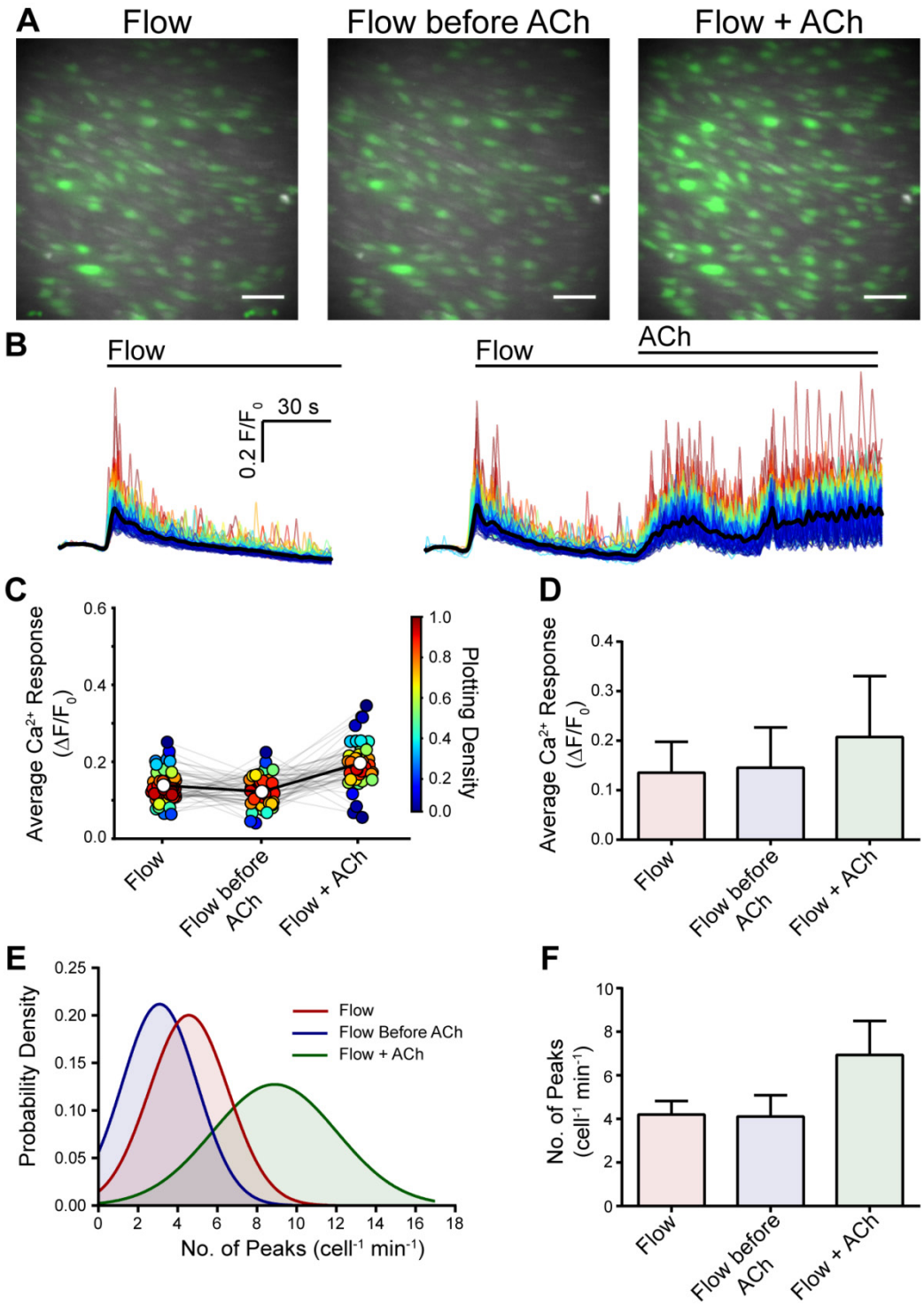

Supplementary Figure S2 Flow-induced endothelial Ca^{2+} signalling (A) Representative composite images of Ca^{2+} activity in carotid artery endothelium in response to stimulation with flow (1.5 ml/min) and ACh (300 nM). The three images show the same field of endothelium from a single experiment. The endothelium was stimulated with flow (A, left panel), flow before the addition of ACh (A, middle panel) and ACh in the presence of a flow-induced response (A, right panel). Scale bars = 50 µm. (B) Ca^{2+} traces corresponding to the datasets shown in A. Ca^{2+} signals are from all 154 activated individual cells are shown. The color assigned to each trace is based on the amplitude of the initial response to flow in each cell i.e. if a cell's trace is colored red in one set of traces, the same trace in the other data sets is also colored red. (C) Average Ca^{2+} ($\Delta F/F_0$) response from each individual cell (circle) matched for each treatment (grey line) from a single experiment. The average response is indicated by white circle and matched across each treatment by bold line. The Plotting Density (right axis) indicates the distribution of average $\Delta F/F_0$ values. (D) Summary data of average Ca^{2+} responses to flow, flow before the addition of ACh and ACh in the presence of flow induced Ca^{2+} signals (n=3). (E) Histogram illustrating the frequency distribution of the number of peaks/cell/minute. (F) Summary data of the number of peaks/cell/minute to flow, flow before the addition of ACh and ACh in the presence of flow induced Ca^{2+} signals (n=3).

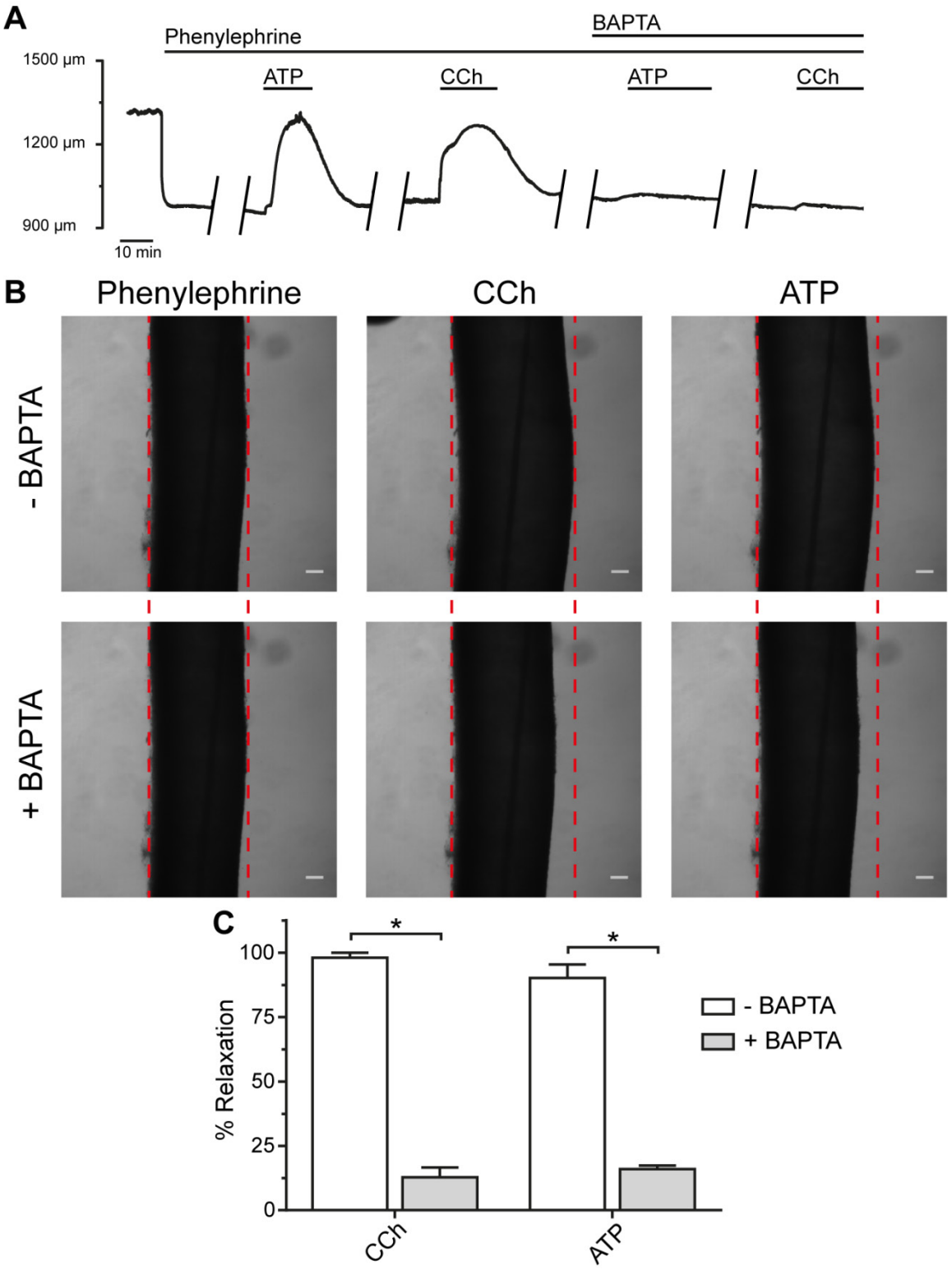

Supplementary Figure S3 Endothelial Ca^{2+}-dependence of CCh- and ATP-evoked relaxation (A) Representative experiment showing the vasorelaxant effects of ATP (100 µM) and CCh (100 µM) on arteries constricted by 20% from their maximal diameter by phenylephrine. Experiments, carried out in the same artery, show the effects of selective buffering of endothelial Ca^{2+} using the cell-permeable selective Ca^{2+}-chelator, BAPTA-AM (30 µM). (B) Brightfield image showing a pressurized carotid artery (110 mmHg) contracted to phenylephrine (left-panel). The middle and right-panels show the same artery under the effects of CCh and ATP as indicated, both in the absence (top row) and presence (bottom row) of BAPTA-AM. The red line indicates the diameter of the artery in the absence of BAPTA-AM at each of the conditions indicated. (C) Summary data showing the vasorelaxant effects of the muscarinic receptor agonist CCh and purinergic receptor agonist ATP on a preconstricted pressurised artery (n = 3, *p < 0.05). All scale bars = 200 µm.

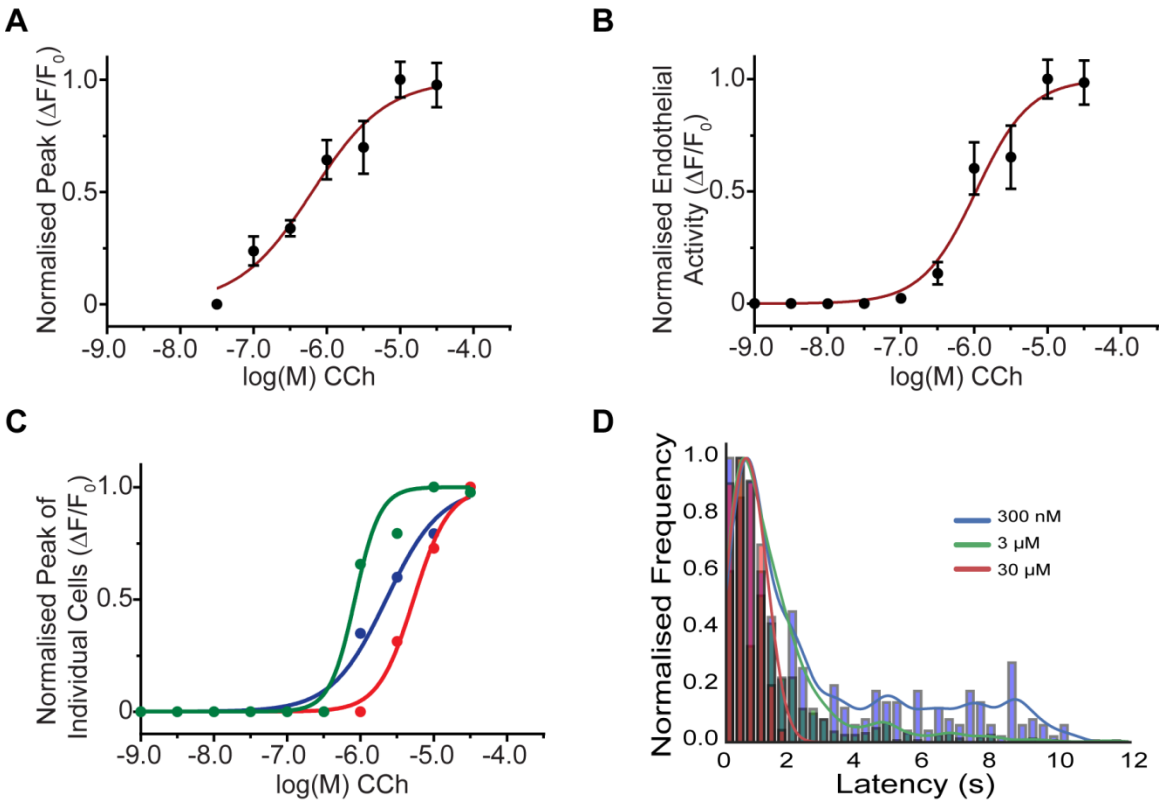

Supplementary Figure S4 Concentration-dependence of the CCh-evoked endothelial Ca^{2+} response. (A-D) Summary data illustrating the concentration dependence of the endothelial response to CCh (n = 5): (A) magnitude of the initial peak ($\Delta F/F_0$) in the Ca^{2+} response to CCh, this data presents average values of cells that responded to each concentration. (B) Concentration dependence of *total* endothelial activity, this data is the overall response averaged across the endothelium, the response of those cells that do not respond is considered zero. The averages of each concentration response were normalized to the maximal response within the experiment; (C) Representative concentration response obtained from three individual cells within a single experiment series. (D) Histograms showing latency distributions. Fitted curves were obtained by Gaussian kernel density estimation.

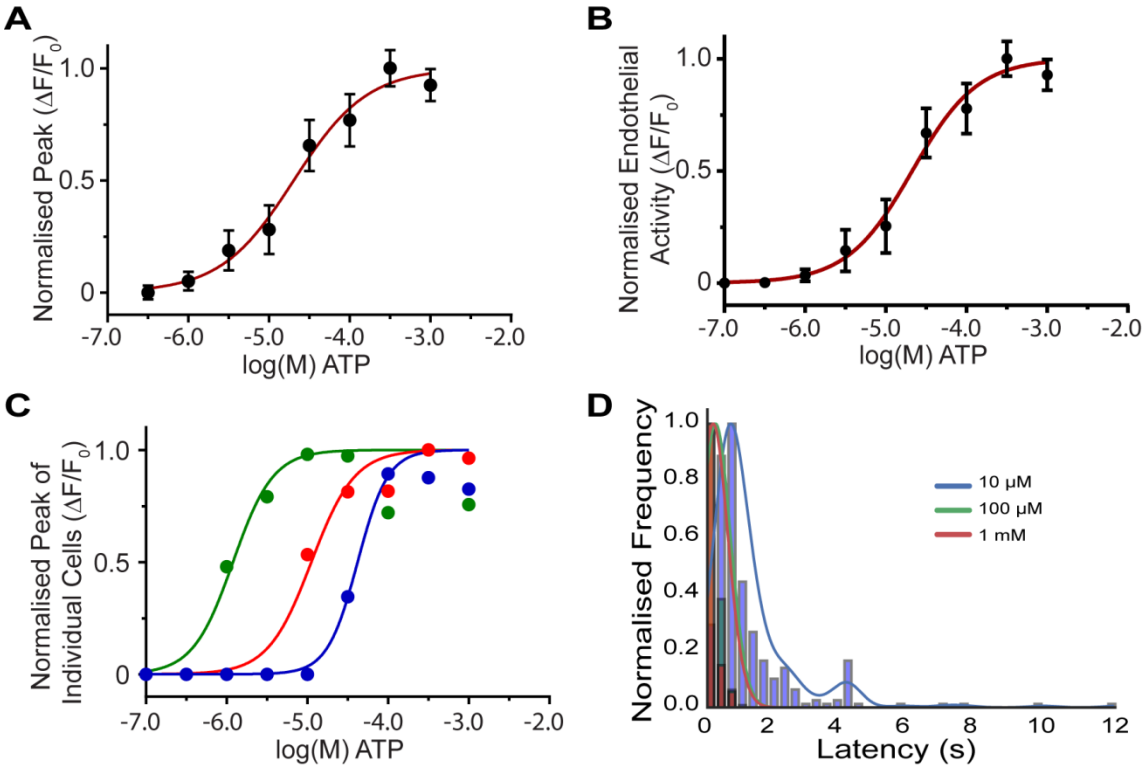

Supplementary Figure S5 Concentration-dependence of the ATP-evoked endothelial Ca^{2+} response. (A-D) Summary data illustrating the concentration dependence of the endothelial response to ATP (n = 5): (A) magnitude of the initial peak ($\Delta F/F_0$) in the Ca^{2+} response to ATP, this data presents average values of cells that responded at each concentration (B) Concentration dependence of *total* endothelial activity, this data represent the overall response averaged across the endothelium, the response of those cells that do not respond is considered zero. The averages of each concentration response were normalized to maximal response within each experiment; (C) Representative concentration response obtained from three individual cells within a single experiment series. (D) Histograms showing latency distributions. Fitted curves were obtained by Gaussian kernel density estimation.

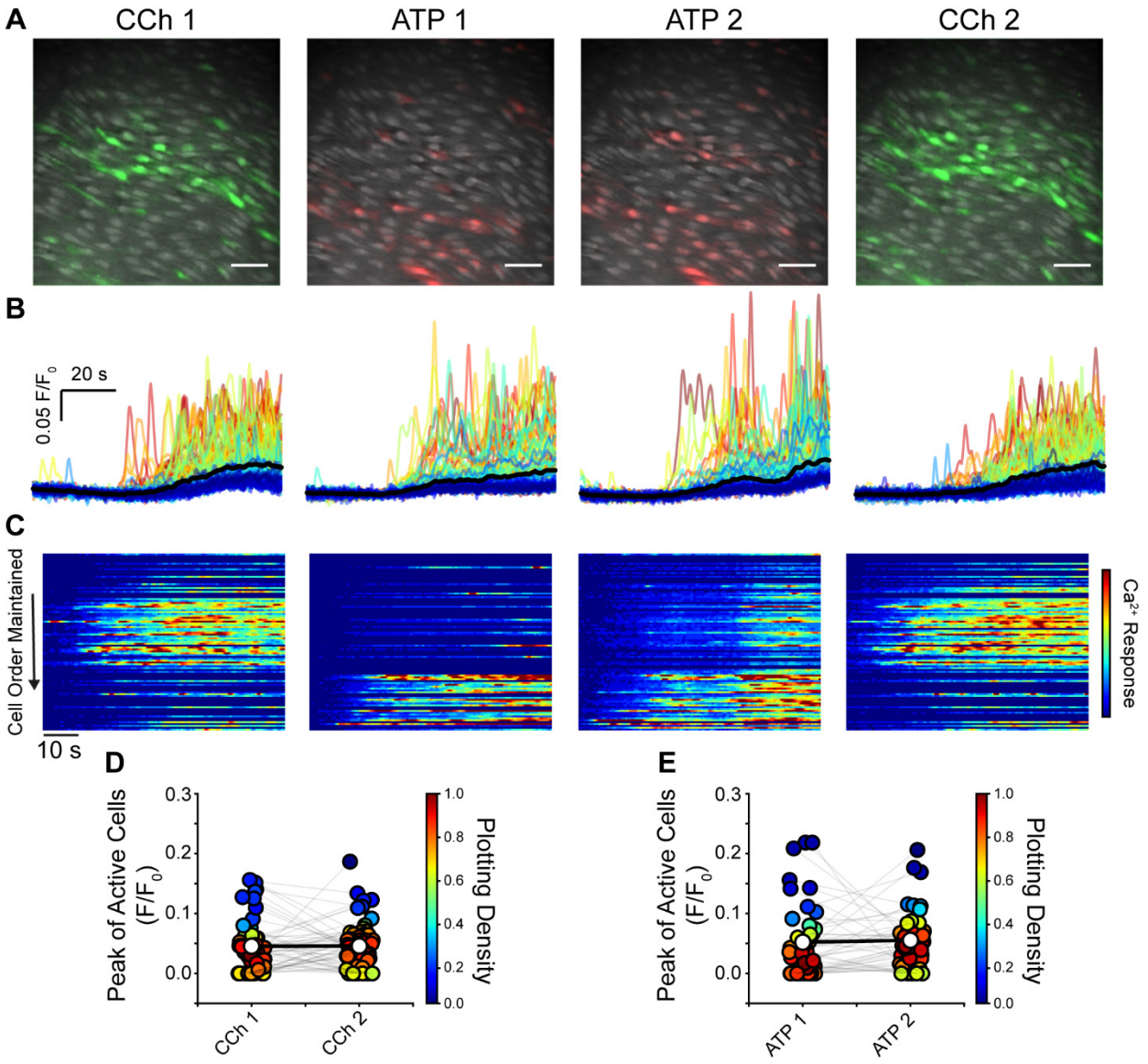

Supplementary Figure S6 The pattern of cell activation is unaltered by sequence of agonist addition (A) Composite Ca^{2+} images showing cells that respond to the EC_{25} concentration of CCh (green) and ATP (red). In the first part of the experiment, CCh was applied and after wash and recovery then ATP (see supplementary Fig 1G for protocol). Next, ATP was applied and after wash and recovery then CCh. All images are from the same field of endothelium. (B) Ca^{2+} responses from the activated cells in A. 30s of baseline and 60s of activation are shown. (C) Heat map showing a combination of all cells that respond to either CCh or ATP. Each row illustrates an individual endothelial cell and the order is maintained across all four treatments. (D-E) Paired data from a single experiment showing the peak F/F_0 values of only the active cells (circles). The Plotting Density (right axis) indicates the distribution of Peak F/F_0 values (red high overlap of values, blue low overlap of values). All Scale bars = 50µm.

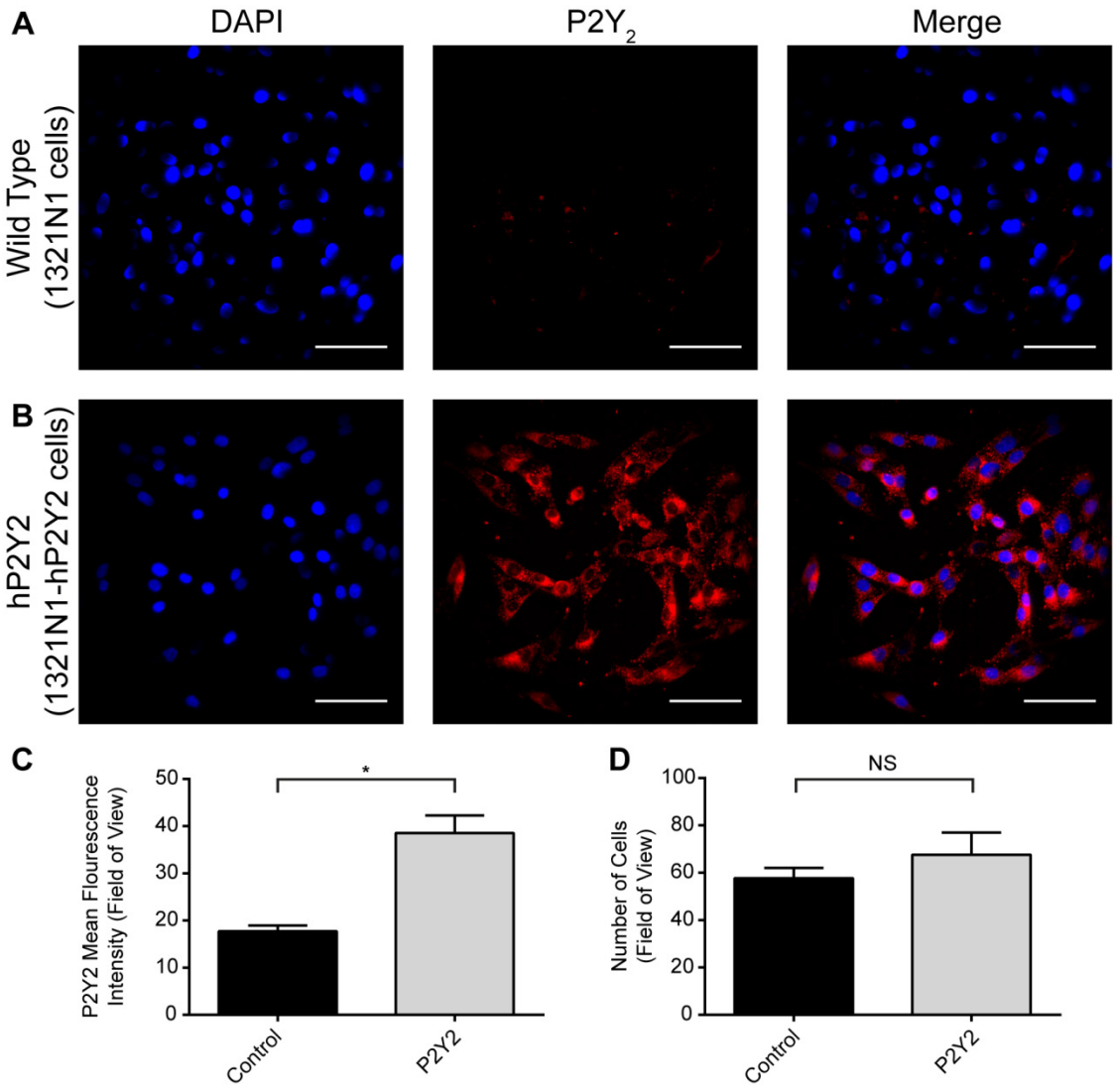

Supplementary Figure S7 Specificity of the P2Y2 receptor antibody (A) Fluorescence localization of purinergic P2Y2 receptors in human astrocytes (1321N1 cells; which lack all eight P2Y subtypes). Representative images (from left) show astrocyte cell nuclei (blue; DAPI), P2Y2 receptor distribution (red; anti-P2Y2) and overlay of both (B) Fluorescence localization of purinergic P2Y2 receptors in 1321N1-hP2Y2 cells which stably express recombinant human hP2Y2 receptors. Representative images (from left) show astrocyte cell nuclei (blue; DAPI), P2Y2 receptor distribution (red; anti-P2Y2) and overlay of both (C) Summary data showing the level of P2Y2 receptor staining in wild-type (black) and hP2Y2 (grey) cells. (D) Summary data showing the number of cells in each field of view. (n = 3, *p < 0.05, unpaired t-test). All scale bars = 50 μm.

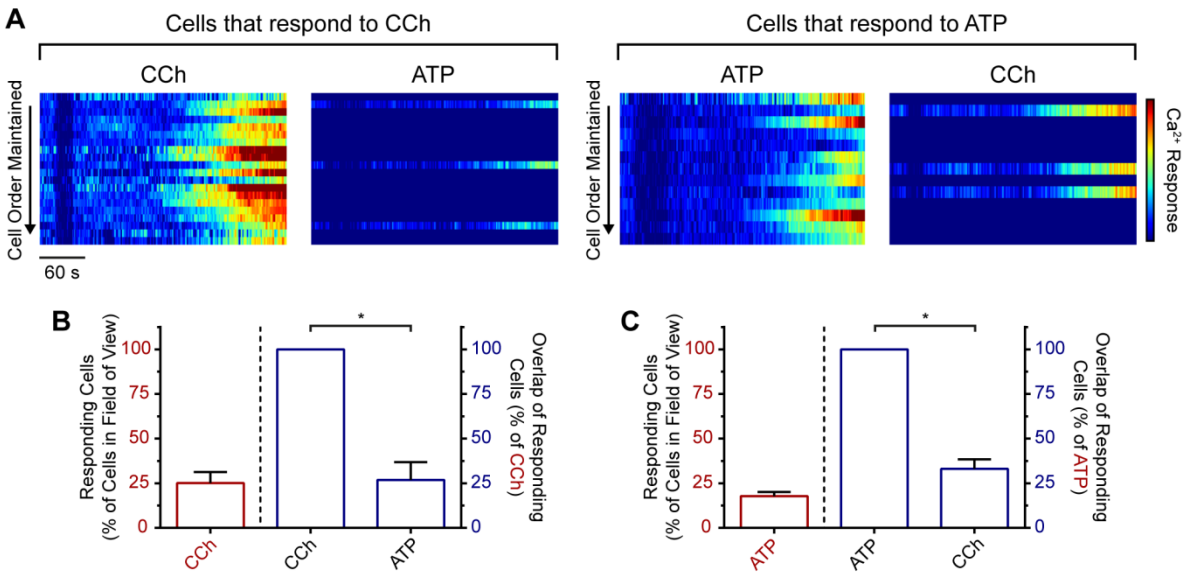

Supplementary Figure S8 Heterogeneity in nitric oxide production (A) Heat map showing the cells (left axis) that respond to the EC_{50} (for Ca^{2+}) of CCh and ATP with nitric oxide production as measured by DAR-4M in the same preparation. Each row in the panels illustrates an individual endothelial cell and the order is maintained across all treatments. (A) left-panels, shows the cells that respond to CCh alone i.e. nitric oxide production in response to CCh but not ATP. (A) right-panels shows the cells that respond to ATP alone i.e. nitric oxide production in response to ATP but not CCh. (B-C) Number of cells activated as a percentage of the total population of cells in the field (red bar, left side). The right side of each plot (B-C, blue bars) shows the percentage of precisely the same cells that are activated by each of the conditions shown on the x axis. The plots show that those cells that are most sensitive to one agonist in producing nitric oxide are much less sensitive to the other agonist (n=3). There is a significant difference in the cells that respond to each agonist ($p<0.05$).